

# Influence of fault trend, bends, and convergence on shallow structure and geomorphology of the Hosgri strike-slip fault, offshore central California

Samuel Y. Johnson and Janet T. Watt

U.S. Geological Survey, 400 Natural Bridges Drive, Santa Cruz, California 95060, USA

## ABSTRACT

We mapped an ~94-km-long portion of the right-lateral Hosgri fault zone in offshore central California using a dense network of high-resolution seismic reflection profiles, marine magnetic data, and multibeam bathymetry. These data document the location, length, and continuity of multiple fault strands, highlight fault-zone heterogeneity, and demonstrate the importance of fault trend, fault bends, and fault convergence in the development of shallow structure and tectonic geomorphology along strike-slip faults.

Eight sections (A through H) of the Hosgri fault are mapped. The fault trends ~335° to 341° in the southern ~40 km of the study area (sections A through C) where shallow deformation is primarily dilational. The absence of tectonic uplift in this area has contributed to localization of the Santa Maria River and delta and, as a result, Holocene sediments cover the fault zone. The Hosgri fault generally trends 329° to 337° in the central ~24 km of the study area (sections D through F), which coincides with oblique convergence of the Hosgri and the more northwest-trending Los Osos and Shoreline faults. This convergence has resulted in local restraining and releasing fault bends, transpressive uplifts, and extensional basins of varying size and morphology. Notably, development of a paired fault bend is linked to indenting and bulging of the Hosgri fault by a strong crustal block translated to the northwest along the Shoreline fault. Two diverging Hosgri fault strands bounding a central uplifted block characterize the northern ~30 km of the Hosgri fault (sections G and H) in this area. The eastern Hosgri passes through significant releasing (329° to 335°) and restraining (335° to 328°) bends before passing onland at San Simeon; the releasing bend is the primary

control on development of an elongate, asymmetric, 15-km-long × 300- to 2400-m-wide, “Lazy Z” sedimentary basin. The western strand of the Hosgri fault passes through a significant restraining bend (329° to 316°) and continues northward until slip is transferred to faults underlying the Piedras Blancas fold belt.

Earthquake hazard assessments should incorporate a minimum rupture length of 110 km based on continuity of the Hosgri fault zone through this area. Lateral slip rates may vary along the fault (both to the north and south) as different structures converge and diverge but are probably in the geodetically estimated range of 2–4 mm/yr.

## INTRODUCTION

The geology of strike-slip fault zones is relatively well known from decades of comprehensive research (e.g., Crowell, 1974; Ballance and Reading, 1980; Biddle and Christie-Blick, 1985; Harding, 1985; Cunningham and Mann, 2007). Dynamic models allow broad characterization about fault geometry and structure in these fault zones, while detailed field mapping commonly highlights complexities associated with multiple fault strands, local domains of extension and contraction, tectonic inversion, and diverse fault-zone histories. Understanding shallow structure in strike-slip zones is especially important because it provides data on recent and active faulting—essential information for earthquake hazard assessment. In most cases, seismic-reflection profiling is the best tool for collecting such shallow, high-resolution structural data.

Onland mapping and structural studies of strike-slip faults are facilitated by overall accessibility and the availability of increasingly higher-resolution topographic data (e.g., Arrowsmith and Zielke, 2009), but high-quality and high-resolution seismic-reflection data are

generally sparse due to both the cost and logistical difficulty of data collection. In contrast, seismic-reflection data are much easier to collect and more available offshore (e.g., U.S. Geological Survey, 2008) but profiles are commonly widely spaced and lack resolution in the shallow subsurface; many such surveys were designed to image deeper (0 to ~6 km) structure and stratigraphy for the purposes of documenting gross geologic framework and/or petroleum resource exploration. We attempt in this paper to combine the efficiencies of working offshore while approaching the resolution of onshore mapping by collection, integration, and analysis of multiple data sets including high-resolution seismic-reflection profiles, multibeam bathymetry, and marine magnetic data.

The target of this investigation is the Hosgri fault, one of the major strike-slip faults in the widely distributed transform plate boundary along the west coast of North America (Hanson et al., 2004; Lettis et al., 2004; Dickinson et al., 2005). We collected ~1500 km of single-channel seismic-reflection data offshore central California between Point Sal and Piedras Blancas, crossing an ~94-km-long portion of the Hosgri fault 121 times. Seismic profiles were integrated with similarly dense marine magnetometer data and high-resolution bathymetric data collected within State Waters (shoreline to 5.6 km offshore) for the California Seafloor Mapping Program (U.S. Geological Survey, 2009). The resulting comprehensive geophysical database documents the location, length, and continuity of multiple fault strands, highlights fault-zone heterogeneity, and demonstrates the importance of fault trend, fault bends, and fault convergence in fault-zone evolution and development of tectonic geomorphology.

## TECTONIC SETTING

The northwest-trending, right-lateral, strike-slip Hosgri-San Gregorio fault system is part

of the widely distributed transform boundary between the Pacific plate and the Sierran microplate (Fig. 1; Argus and Gordon, 2001). The San Andreas fault is the primary structure within this boundary, with an estimated slip rate in central California (Carrizo Plain) of ~30–36 mm/yr and a trend of ~319° (Sieh and Jahns, 1984; Argus and Gordon, 2001; McCaffrey, 2005; Meade and Hager, 2005; Titus et al., 2011).

Faults in central California west of the San Andreas fault accommodate a geodetically estimated additional ~4–5 mm/yr of dextral slip (Argus and Gordon, 2001; McCaffrey, 2005; Meade and Hager, 2005). The Hosgri-San Gregorio fault system, the most extensive of these western structures, extends ~400 km

along the central California coast (Fig. 1; Hanson et al., 2004; Lettis et al., 2004; Dickinson et al., 2005). At its south end, the Hosgri fault initiates at the northern boundary of the western Transverse Range province offshore Point Arguello (Steritz and Luyendyk, 1994; Sorlien et al., 1999). As it extends north, this mainly offshore fault system intersects the Big Sur coast at Piedras Blancas and at Point Sur where strands are referred to as the San Simeon and Sur faults. Farther north, the fault system emerges in the Monterey Bay area as the San Gregorio fault zone (Greene et al., 2002), which continues to the north and merges with the San Andreas fault offshore San Francisco (Bruns et al., 2002; Ryan et al., 2008).

Hanson and Lettis (1994) presented onshore geologic data (offset marine terrace strandlines and drainages) from Piedras Blancas (Fig. 1) that suggest lateral slip rates of 0.4–11 mm/yr with best estimates in the 1–3 mm/yr range. Farther north, Weber (1994) estimated a slip rate of ~4–10 mm/yr for the San Gregorio fault near Point Año Nuevo south of San Francisco (Fig. 1). The Working Group on California Earthquake Probabilities (Wills et al., 2008) uses preferred slip rates of 2.5 mm/yr for the Hosgri fault zone and 3–7 mm/yr for the San Gregorio fault zone.

This investigation focuses on an ~94-km-long region of the coast between Point Sal and Piedras Blancas (Fig. 2). In this region, the Hosgri fault forms the eastern margin of the offshore Santa Maria basin, which has accumulated as much as 3 km of predominantly fine-grained, Neogene marine strata (McCulloch, 1987). To the east, the Hosgri fault bounds the “Los Osos Domain” of Lettis et al. (2004), a triangular region bounded by the west-trending Santa Ynez River fault (northern flank of Western Transverse Range province) on the south and the northwest-trending Oceanic-West Huasna fault zone on the northeast (Fig. 1). This structural domain includes several northwest-trending faults that converge with the Hosgri fault zone in the study area, including the Lions Head fault, Casmalia fault, Los Osos fault, and Shoreline fault (Fig. 2; Lettis et al., 2004; Hardebeck, 2010).

## DATA ACQUISITION

Approximately 1500 km of single-channel seismic-reflection data were collected by the U.S. Geological Survey (USGS) between Piedras Blancas and Point Sal in 2008, 2009, and 2011 (Fig. 2; Sliter et al., 2009). Data were mostly acquired on N60°E-trending profiles perpendicular to the Hosgri fault. Profile spacing is typically 800 m apart (locally 400 m), and the fault zone was crossed 121 times. Numerous shore-parallel tie lines were also collected. Data were acquired using a 500 J mini-sparker source fired at a 1/2 s shot interval and a 15-m-long hydrophone streamer. The source signal frequency bandwidth ranges from ~200 to 1600 Hz. Data quality varies with substrate, ranging from as much as 200 to 300 m of penetration in inferred Quaternary marine deposits to as little as 0 m in heterogeneous Mesozoic basement.

Marine magnetic data were collected on the same surveys using the Geometrics G882 cesium vapor magnetometer, merged with onland data collected by fixed-wing aircraft (Langenheim et al., 2009) and helicopter (Langenheim et al., 2012), then gridded to 50 m

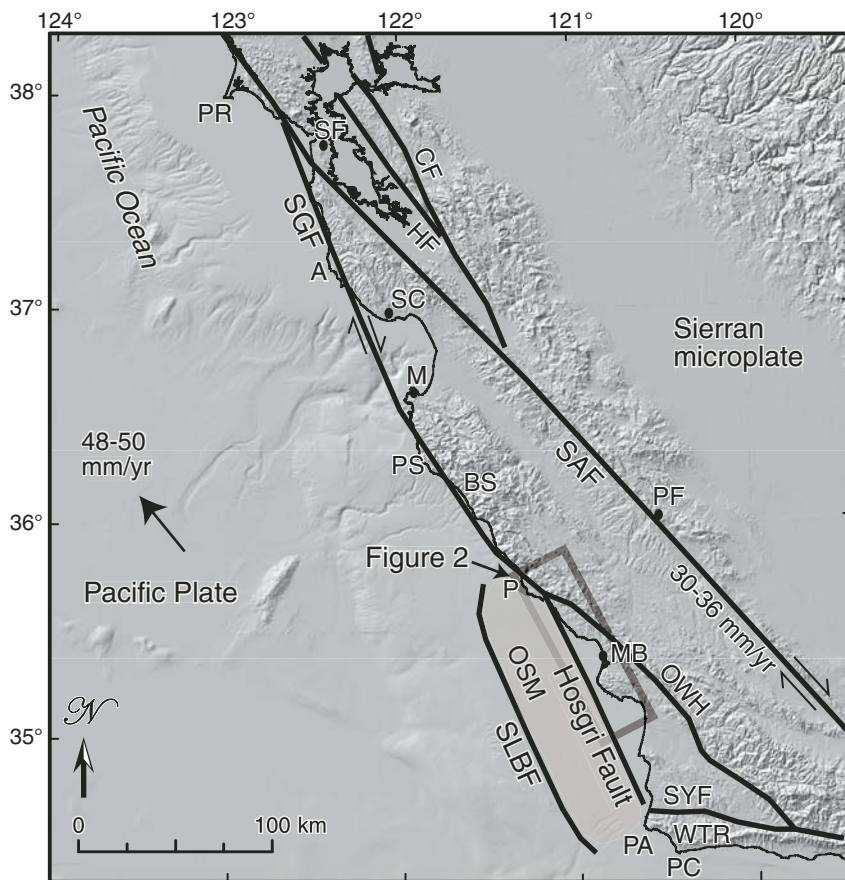


**Figure 1. Regional digital elevation model and index map showing significant faults along the central California coast from Point Conception (PC) to Point Reyes (PR). The Hosgri-San Gregorio fault system lies west of and accommodates some of the relative plate motion (48–50 mm/yr) not taken up by the San Andreas fault (30–36 mm/yr). Box shows area of Figure 2. Abbreviations: A—Point Año Nuevo; BS—Big Sur; CF—Calaveras fault; HF—Hayward fault; M—Monterey; MB—Morro Bay; OSM—Offshore Santa Maria basin (shaded light brown); OWH—Oceanic-West Huasna fault; P—Piedras Blancas; PA—Point Arguello; PF—Parkfield; PS—Point Sur; SAF—San Andreas fault; SC—Santa Cruz; SGF—San Gregorio fault; SF—San Francisco; SGF—San Gregorio fault zone; SLBF—Santa Lucia Bank fault; SYF—Santa Ynez fault; WTR—Western Transverse Ranges.**



7125, 240 kHz Reson 8101, and SEA Swath-Plus). Most of the data were acquired for the California Seafloor Mapping Program (CSMP) and extend from the ~10 m isobath to 5.6 km (3 nautical miles) offshore, the limit of California's State Waters. The CSMP database, along with information on data collection and processing is available at CSUMB (2010). Spatial resolution is typically 1 m in water depths <50 m and 2 m for water depths >50 m.

## INTERPRETATION OF SEISMIC-REFLECTION DATA

Seismic-reflection data are the primary database for documenting shallow structure and stratigraphy. Faults are identified based on the abrupt truncation or warping of reflections, and/or juxtaposition of reflection panels with different seismic parameters such as reflection presence, amplitude, frequency, geometry, continuity, and vertical sequence. The Hosgri fault zone commonly includes several distinct splays, of which the more continuous faults and those that bound sedimentary basins are considered the primary structures. Folding is common throughout the study area and well imaged on seismic-reflection profiles when dips are less than ~30°.

Four basic stratigraphic units are imaged on the seismic-reflection and bathymetric data. Two older units (below) comprise Mesozoic basement and Neogene marine rocks; their presence is largely extrapolated from onshore mapping of Hall (1973, 1976), Hall and Prior (1975), Hall et al. (1979), and Dibblee and Ehrenspeck (1989). Two younger units consist of Quaternary sediments. The seismic-stratigraphic nomenclature used below is after Mitchum et al. (1977).

(1) Mesozoic basement rocks include Jurassic Coast Range Ophiolite; Jurassic to Cretaceous Franciscan Complex mélange, metavolcanic rocks, and serpentinite; and Cretaceous sandstone. These complexly deformed rocks are generally "reflection-free" (i.e., massive) on seismic-reflection profiles and form rough, irregular, lumpy seafloor outcrops on high-resolution bathymetric imagery.

(2) Neogene marine rocks include tuffaceous sandstone and siltstone of the Miocene Obispo Formation, siliceous and carbonaceous mudstone of the Miocene Monterey Formation, and sandstone and siltstone of the Pliocene Pismo Formation. On seismic-reflection profiles, these strata yield parallel, continuous, low amplitude, high-frequency reflections. Neogene strata were folded and uplifted in the Pliocene (Clark et al., 1991; Hanson et al., 2004) and form differentially eroded seafloor outcrops on high-resolution bathymetric imagery; these distinctly

"ribbed" outcrops facilitate mapping of folds and faults.

(3) Inferred Quaternary sediments overlie a Pliocene unconformity (Hanson et al., 2004) and underlie a transgressive erosion surface ( $\leq$  ca. 20 ka) associated with the latest Pleistocene sea-level rise. These strata are typically characterized on seismic-reflection profiles by continuous, parallel to subparallel, moderate to high amplitude, high-frequency reflections. Prograding clinoforms also underlie the shelfbreak and upper slope in the central part of the study area. This unit occurs beneath the present shelf and slope and was presumably deposited in similar shelf and slope environments during high sea-level stands (Fig. 3) when stratigraphic accommodation space was greatest (e.g., Catuneanu, 2006). Given the potential for uplift and erosion within and adjacent to the Hosgri fault zone (see below) during the Quaternary, it is likely that much of the upper part of this unit beneath the shelf and in local, fault-bounded basins formed during Marine Isotope Stage 5 (ca. 130–71 ka), the most recent, long, sea-level highstand. The presence of local internal angular and/or erosional unconformities in some fault-bounded basins suggests longer Quaternary depositional histories (pre-dating Stage 5), as do thicker accumulations of inferred Quaternary strata beneath the upper slope. Quaternary strata are typically covered by latest Pleistocene to Holocene deposits (see below) and rarely crop out at the seafloor.

(4) Latest Pleistocene to Holocene (< ca. 20 ka) strata are the youngest and uppermost unit on seismic-reflection data, deposited during the

time that sea level rose ~125–130 m following the Last Glacial Maximum (LGM; Mix et al., 2001; Clark et al., 2009). On seismic profiles, these strata are typically characterized by low- to moderate-amplitude, low- to high-frequency, parallel, continuous to moderately continuous reflections. The contact with underlying units is a transgressive surface of erosion commonly marked by angularity, channeling, or a distinct upward change to lower amplitude, more diffuse reflections. Since the shelf was partly emergent during the post-LGM rise, the lower part of the unit may in places consist of thin marginal marine sediments deposited as sea level rose and the shoreline migrated landward. The upper part of this unit consists of marine strata similar to the sediments that are presently being deposited. Similar post-LGM facies overlying a transgressive surface of erosion have been described elsewhere along the central California coast (e.g., Anima et al., 2002; Grossman et al., 2006; Draut et al., 2009).

In addition to providing structural and stratigraphic information, seismic-reflection (and bathymetric) data reveal that the modern shelfbreak generally occurs at depths of ~118–130 m, correlating with the Stage 2 sea-level lowstand (Fig. 3). This shelfbreak occurs at a lateral change from the gently dipping (0.8° to 1.0°) outer shelf to the more steeply dipping (~1.5° to 2.5°) upper slope, and the outer shelf is considered a partly buried, lowstand, wave-cut platform. The shelfbreak is not present south of Port San Luis (Figs. 2 and 4), where seismic data show that prograding deltaic deposits of the Santa Maria River form a continuous low-angle

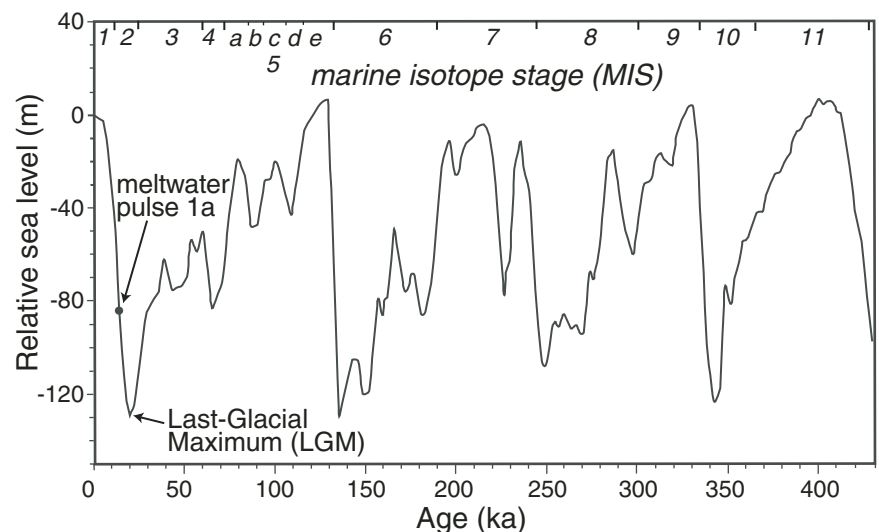


Figure 3. Late Quaternary sea-level curve based on Wright (2000), Waelbroeck et al. (2002), and Peltier (2005).

( $\sim 0.8^\circ$ ) ramp that extends to water depths of more than 160 m.

At the surface or at shallow depths, seismic profiles have also imaged submerged and partly buried paleo-shorelines. Post-LGM sea-level rise and landward shoreline migration were not steady but rather characterized by periods of relative stability and rapid submergence (e.g., Peltier, 2005). During  $\sim 14$  ka Meltwater Pulse 1A (Fig. 3), for example, sea level rose  $\sim 20$  m in 200–500 years. Such pulses rapidly submerge wave-cut platforms,

shorelines, and shoreline angles (Kern, 1977) increasing the potential for their preservation.

### HOSGRI FAULT ZONE CHARACTERIZATION

We have mapped the Hosgri fault between Point Sal and Piedras Blancas through integration of comprehensive high-resolution seismic-reflection and marine magnetic data, and high-resolution bathymetry where avail-

able (Fig. 2). Based on this mapping, we divided the Hosgri into eight “sections” (“A” through “H”) distinguished on the basis of fault trend, shallow structure and stratigraphy, and seafloor geomorphology.

Previously Hanson et al. (2004, see their fig. 2) defined four “reaches” of the Hosgri fault in the central and southern part of this area based on changes in fault geometry and structure. These “reaches” correlate with the “sections” we delineate as follows: The *Point Sal reach*

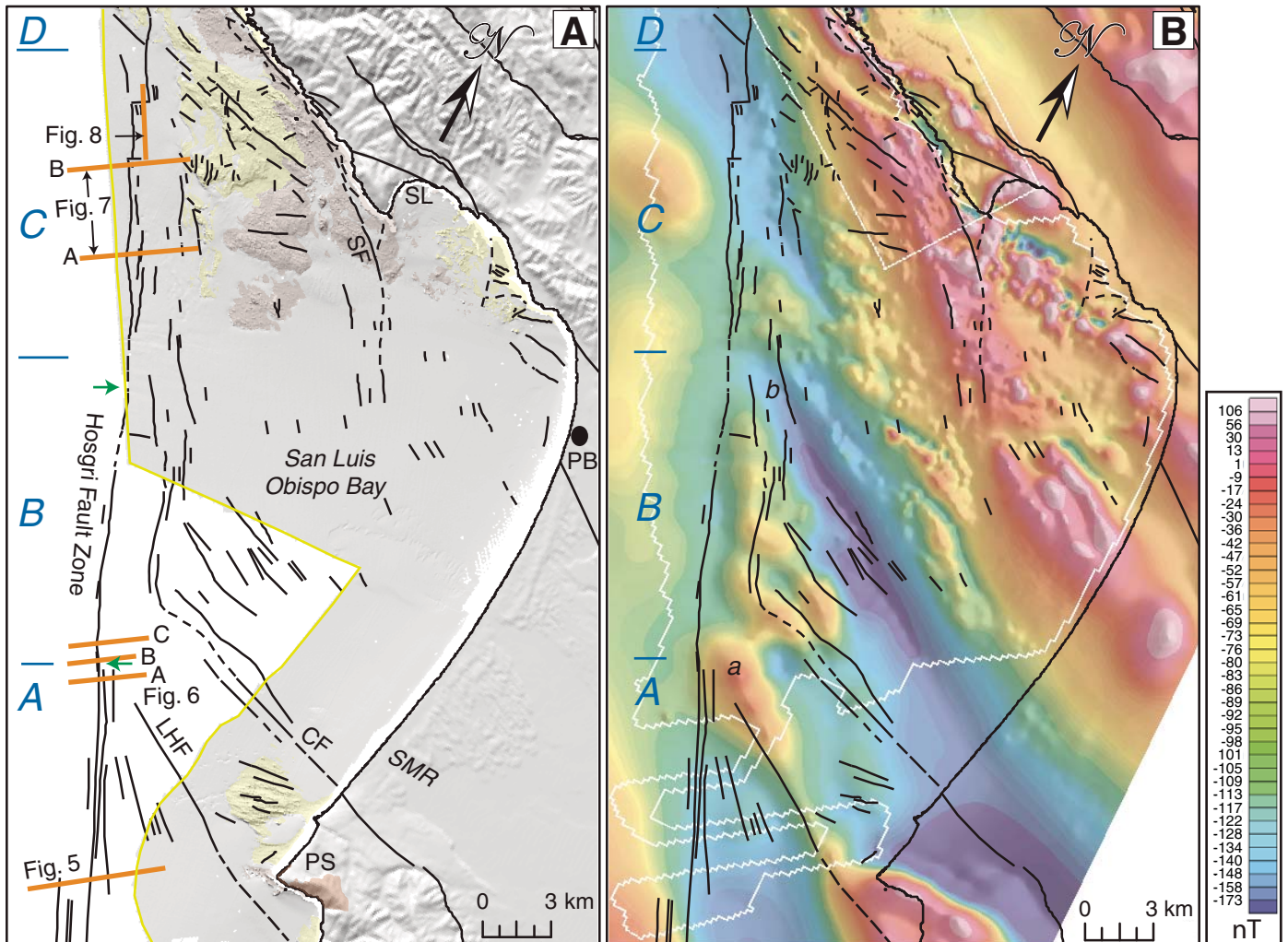


**Figure 4.** Southern part of study area between Point Sal (PS) and Port San Luis (SL). Black lines show faults mapped with shallow seismic-reflection data (offshore) and from U.S. Geological Survey and California Geological Survey (2010) onshore. Blue letters indicate Hosgri fault sections (A, B, C, D). (A) Hillshade showing onshore-offshore relief; gray white boundary shows the boundary of available multibeam bathymetry. Pale brown and pale yellow polygons show seafloor outcrops of Mesozoic and Neogene bedrock; brown polygon onshore at Point Sal shows location of Point Sal Ophiolite (Hopson, 2007). Orange bars show locations of seismic-reflection profiles in Figures 5–8. Green arrows show approximate locations of gradual fault bends. The area lies offshore of the mouth of the Santa Maria River (SMR), a major sediment source. Other abbreviations: CF—Casmalia fault; LHF—Lions Head fault; PB—Pismo Beach; SF—Shoreline fault. (B) Hillshaded magnetic anomaly grid (50 m) based on data in Sliter et al. (2009) and Langenheim et al. (2009). The area noted a is a northwest-trending magnetic high that coincides with the boundary between sections A and B, and b is northwest-trending magnetic trough that terminates northward at the boundary between sections B and C. White lines show boundaries of different magnetic surveys. Note that maps have been rotated  $26^\circ$  from north.

of Hanson et al. (2004) includes the southern part of our section A. The *San Luis Obispo Bay reach* includes the northern part of our section A, all of section B, and the southern part of section C. The *San Luis/Pismo reach* includes the northern part of section C, all of sections D and E, and the southern part of section F. The *Northern reach* includes the northern part of section F and the southern part of section G. The northern part of section G and all of section H of this paper lie north of the *Northern reach* of Hanson et al. (2004).

**Section A**

Section A of the Hosgri fault zone strikes northwest (336°) for ~12.5 km from offshore Point Sal at the south end of our map area (Figs. 2 and 4). The fault section lies parallel to a moderate to locally steep magnetic gradient that changes polarity from south (higher to the west) to north (higher to the east). The northern end of section A coincides and truncates the more west-trending (~305°) projection of a prominent magnetic high (“a” on Fig. 4B) that aligns with the Lions Head fault and the southwest flank of the Point Sal ophiolite (Sylvester and Darrow, 1979; Lettis et al., 2004; Hopson, 2007).

The Hosgri fault zone in section A underlies the Santa Maria River delta and is buried by an offshore-thinning wedge of post-LGM (latest Pleistocene and Holocene) sediment with inferred thickness ranging from ~10 m to 40 m (unit “H” on Figs. 5 and 6A). The base of the post-LGM unit is typically cut or warped by

shallow Hosgri faulting, which is concentrated in a near-vertical zone that varies in width from 200 (Fig. 6A) to 1000 m (Fig. 5).

Structurally controlled sedimentary basins of inferred late Quaternary age (see above) underlie the post-LGM unit on both the west (Figs. 5 and 6A) and east (Fig. 6A) sides of the fault zone. The basin fill consists of flat to gently dipping strata that rest with angular unconformity (local onlap and buttressing) above more steeply dipping basement rocks of inferred Neogene age. On Figure 5, the floor of the Quaternary basin immediately west of the Hosgri fault zone is ~53 m lower than the top of the non-reflective bedrock uplift in the fault zone. Farther north (Fig. 6A), the base of the Quaternary section both east and west of the Hosgri fault zone is more than 16 m lower than the top of the inferred bedrock uplift within the fault zone.

Associated faulting and folding is distributed more broadly in a zone as wide as 3000 m (Figs. 5 and 6A). Active “growth folding” is indicated by stratigraphic thinning over anticlinal axes and thickening in synclines and basinal troughs. On Figure 5, for example, there is ~33 m of stratigraphic thinning over the axis of the gentle anticline in the basin west of the fault zone between reflection “1” and the basal basin reflection. On Figure 6A, fold growth west of the Hosgri fault is at least 55 m as indicated by the difference in thickness between reflections “1” and “2” crossing the anticlinal crest and basinal trough. Thus there is evidence for both Quaternary extension (basin subsidence) and contraction (folding) adjacent to the Hosgri fault zone in section A.

Constraining rates of deformation requires information on ages for which stratigraphic inference is the only guide. As noted above, we infer a post-LGM age for unit “H” in Figures 5 and 6 because (1) it is stratigraphically continuous with the modern seafloor, (2) it is underlain locally by an angular unconformity or transgressive surface of erosion, and (3) seismic facies are consistent with shelf deposition (e.g., Sangree and Widmier, 1977). Accordingly, the rate of vertical offset along the western strand of the Hosgri zone shown in Figure 5 is ~0.3–0.4 mm/yr (6–8 m in 20,000 years). For the truncated anticline shown in Figure 6A, vertical offset adjacent to the eastern fault in the zone is only 0.1 mm/yr (~2 m in 20,000 years). It is emphasized that fault offsets and folding are localized and highly variable on both sides of the fault and that inferred vertical deformation rates vary significantly from profile to profile.

**Section B**

Section B of the Hosgri fault zone extends north-northwest for ~14 km with a trend of 340°–341°, ~4° to 5° more northerly than the fault trend in section A. The fault zone follows a low- to moderate-magnetic gradient (Fig. 4B) and is generally characterized by a single fault or two closely spaced vertical faults (e.g., Fig. 6B) a few hundred meters wide. The northern end of section B (transition to section C) coincides with the projection of a steep, narrow, northwest-trending magnetic trough (“b” on Fig. 4B).

Strata bounding the Hosgri fault zone in section B exhibit parallel, moderate amplitude,

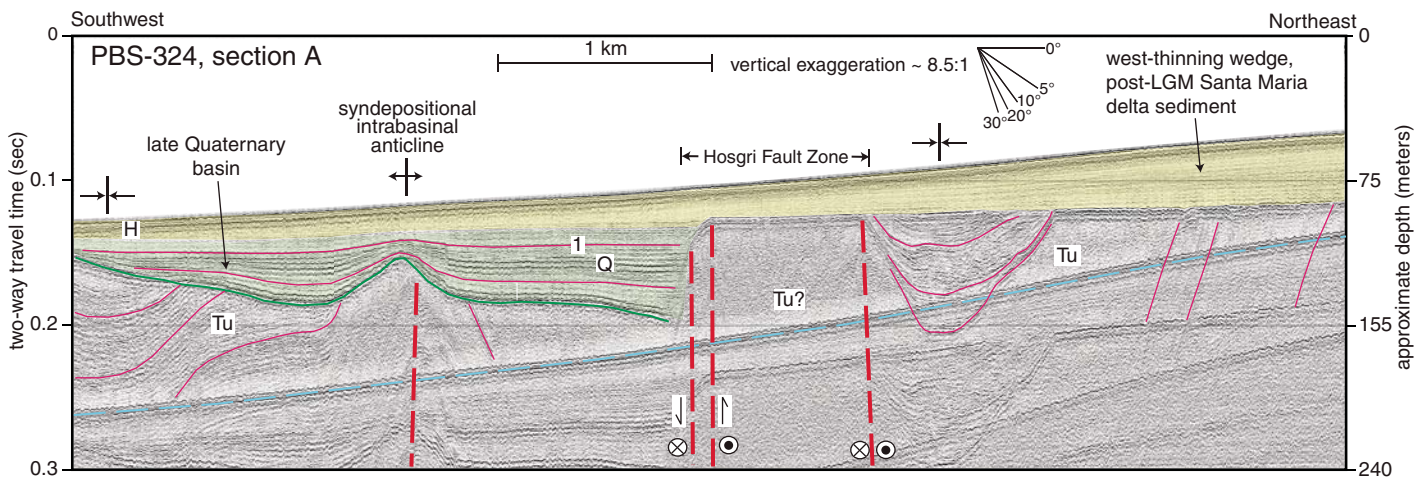


**Figure 5.** USGS seismic-reflection profile PBS-324 offshore Point Sal (location shown in Fig. 4A). Yellow shading shows latest-Pleistocene to Holocene (H) deposits; green shading shows inferred late Quaternary (Q) deposits; Tu—inferred Neogene bedrock. Red dashed lines show faults; green line shows angular unconformity; thin magenta lines (including 1, discussed in text) highlight prominent reflections; blue dashed line shows seafloor multiple. On this and following seismic-reflection profiles (Figs. 6, 7, 10–12, 15, and 17), circles with dots indicate strike-slip motion toward the reader, and circles with x’s indicate motion away from the reader.

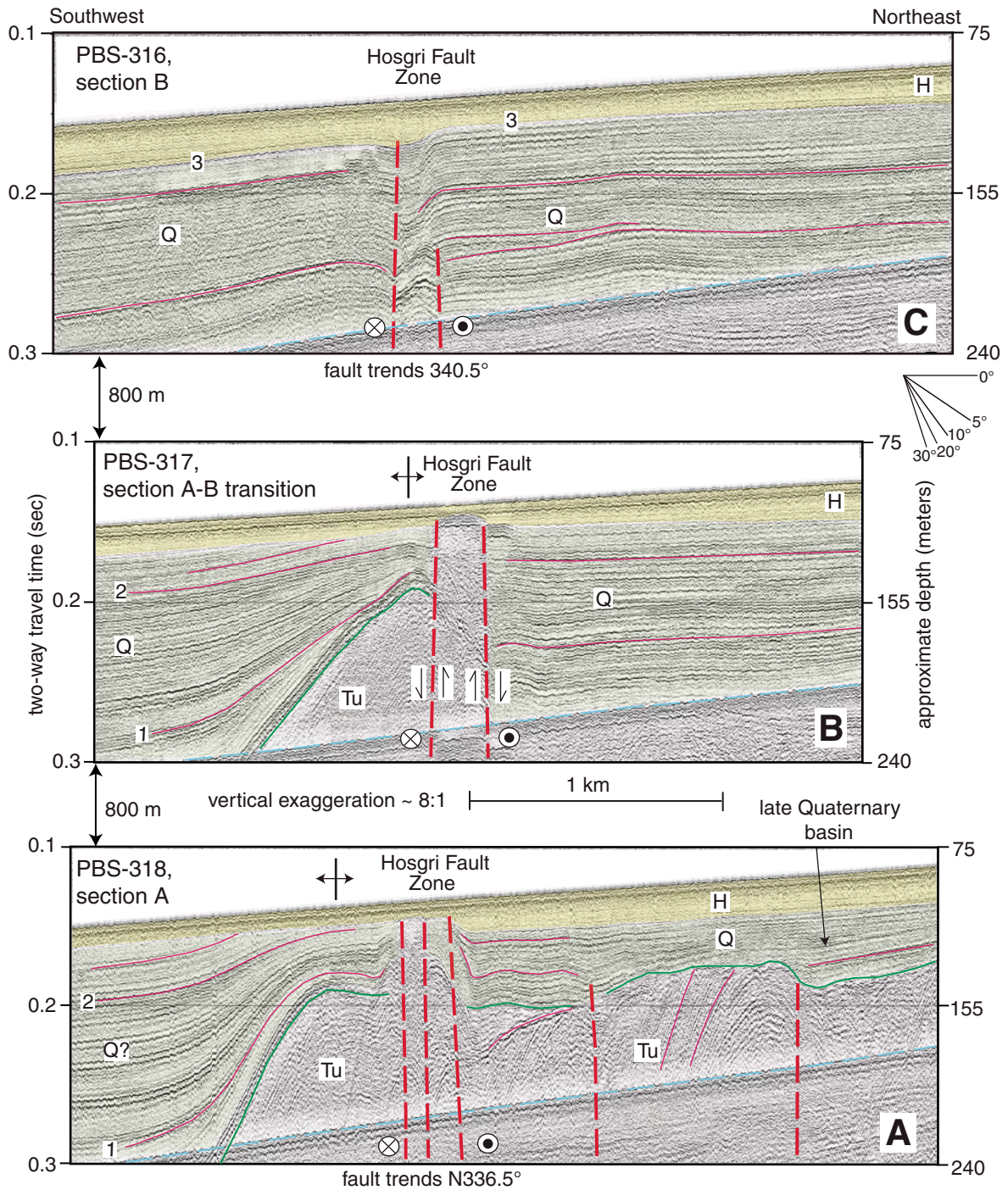


**Figure 6.** USGS seismic-reflection profiles PBS-316, 317, and 318 offshore Point Sal (location shown in Fig. 4A). Yellow shading shows latest-Pleistocene to Holocene (H) deposits; green shading shows inferred late Quaternary (Q) deposits; Tu—inferred Neogene bedrock. Red dashed lines show faults; green line shows angular unconformity; thin magenta lines (some are numbered and discussed in text) highlight prominent reflections; blue dashed line shows seafloor multiple.

high-frequency reflections characteristic of shelf deposits (e.g., Sangree and Widmier, 1977). These strata are inferred to be of late Quaternary age, sourced primarily by the nearby Santa Maria River (Fig. 4A). The fault(s) typically juxtaposes panels of flat-lying to very gently warped strata, an overall structural style that suggests subsidence on both the east and west sides of the Hosgri fault zone. Distinctive marker horizons within these strata that could be used as piercing points to constrain recent vertical deformation either are not obvious or suggest small offsets (0 to ~6 m) with different profiles revealing both west-side-down and east-side-down geometry and no uniformity.

There is a significant change in shallow structure from section A to B. Figure 6A at the north end of section A shows uplifted bedrock and complex, distributed faulting and folding on

both sides of the Hosgri fault zone. Figure 6B, 800 m to the north at the transition from section A to B, reveals similar bedrock uplift and gentle folding west of the fault zone but subsidence and flat-bedded Quaternary strata east of the fault zone. Figure 6C, the profile 800 m north of Figure 6B, reveals a simple fault zone with flat-bedded Quaternary strata on both sides of the fault and a gentle sag in the fault zone. The vertical sequence, amplitude, and frequency of reflections do not match across the fault on the Figure 6C profile, consistent with lateral offset.

The abrupt (over 1600 m) change in shallow structure from section A (Fig. 6A) to B (Fig. 6C) is attributed to the 4° to 5° change in fault trend. This “releasing bend” (e.g., Christie Blick and Biddle, 1985; Mann, 2007) appears to be forming around a rigid, northwest-trending basement block of the Point Sal ophiolite represented by the magnetic high “a” on Figure 4B.

**Section C**

Hosgri fault zone section C is 12.8 km long and extends through a linear magnetic low (Fig. 4B). In this section, the Hosgri fault zone comprises two to three parallel, vertical strands and ranges in width from ~150 m to 1000 m (Fig. 7). The transition from section B to C coincides with a change in the trend of the main fault strand from ~340° to 334°, a gentle restraining bend that is reflected in increasing contractional, shallow deformation in and adjacent to the fault zone (Fig. 7). Mapping also indicates the presence of two right (releasing) steps that offset the zone eastward roughly 200–250 m and 1000–1050 m (Fig. 4). The northern step is crossed by a north-northeast–trending seismic reflection profile that reveals south-side-down normal offset (Fig. 8).

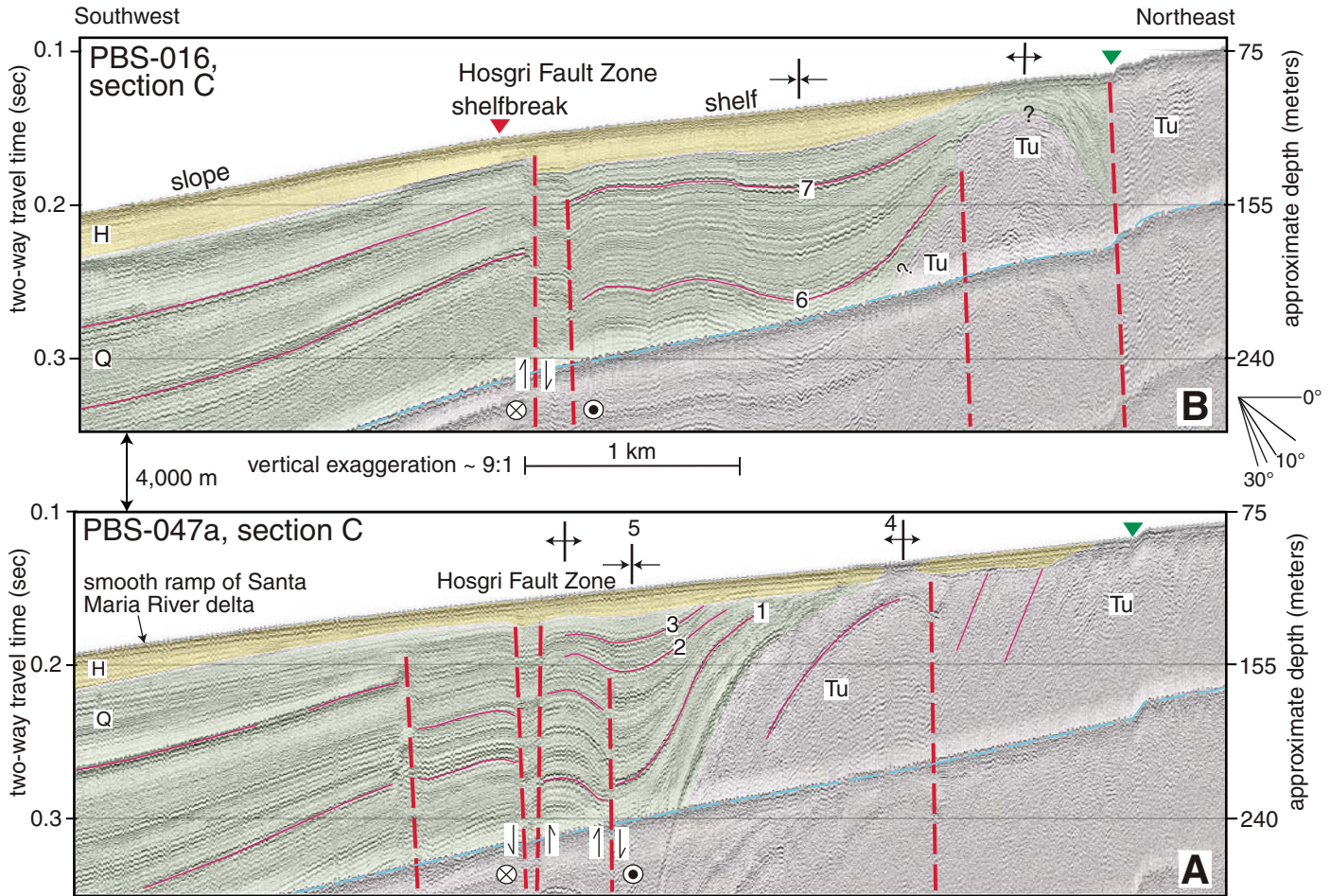


**Figure 7.** Interpreted USGS seismic-reflection profiles PBS-047a and PBS-016, offshore Port San Luis (Figs. 2 and 4). Yellow shading shows latest Pleistocene to Holocene (H) deposits; green shading shows inferred late Quaternary (Q) deposits; Tu—*inferred Neogene bedrock*. Red dashed lines show faults; thin magenta lines (some numbered and discussed in text) highlight prominent reflections; green triangles show notches in seafloor interpreted as paleo-shoreline angle (e.g., Kern, 1977); red triangle shows shelf break—to the south, this geomorphic feature has been draped by Santa Maria River delta deposits. Blue dashed line shows seafloor multiple.

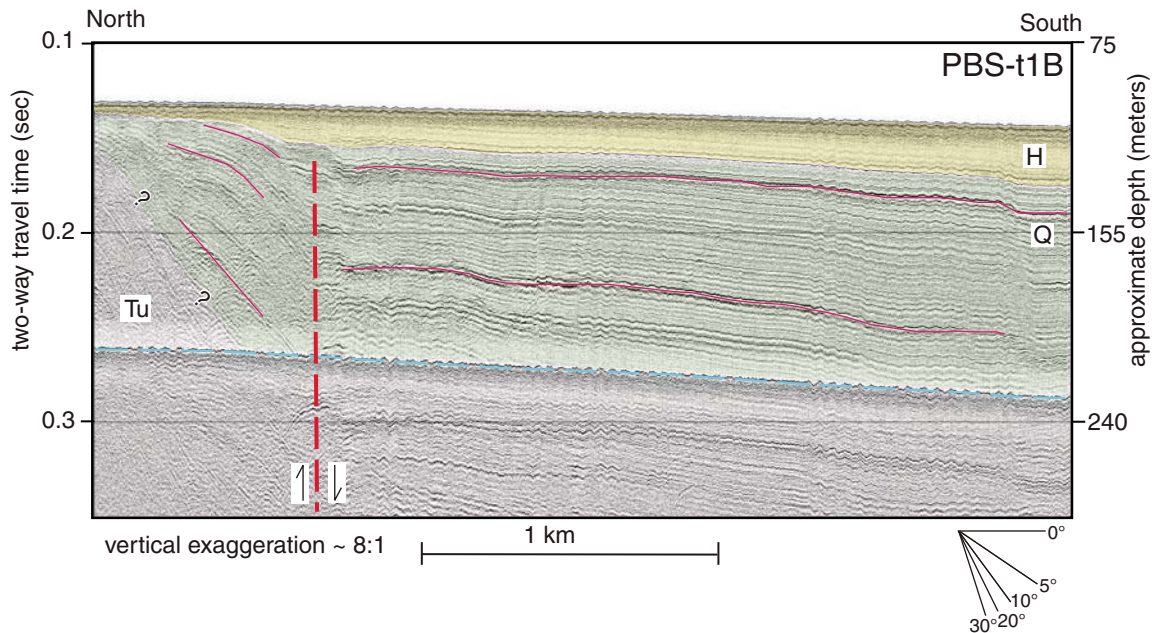


**Figure 8.** Interpreted USGS seismic-reflection profile PBS-t1B, offshore Port San Luis (Figs. 2 and 4). Yellow shading shows latest Pleistocene to Holocene (H) deposits; green shading shows inferred late Quaternary (Q) deposits; Tu—inferred Neogene bedrock. Red dashed line shows normal fault inferred to form at releasing stepover in Hosgri fault zone. Thin magenta lines highlight prominent reflections. Blue dashed line shows seafloor multiple.

Figure 7 shows representative seismic-reflection profiles of section C. Figure 7A shows four vertical faults in a broad (~900 m) zone, while Figure 7B shows two faults in a narrow zone (~150 m). Both profiles reveal the fault zone cutting a thick (>100 m) section of inferred Quaternary strata (“Q”), truncating and warping subhorizontal reflections that cannot be obviously matched across the zone. Vertical offset affecting the post-LGM (ca. 20 ka) section is inferred to be a few meters or less in Figure 7A, but ~10 m (down to the east) in Figure 7B indicating local vertical offset of 0.5 mm/yr.

Growth folding reveals that deformation is distributed across a broad (>2 km) zone east of the Hosgri fault in section C. On Figure 7A, the strata between reflections “1” and “2” thin substantially (from 58 m to 13 m), indicating significant growth of the “4” anticline, and/ or asymmetric subsidence, focused in the “5” synclinal trough. Strata between reflections “2” and “3” likewise thin from 15 m to 8 m across these structures, showing that marked stratigraphic thinning extends upward to the top of the “Q” section. Along-strike variability is revealed by the smaller amount of intrastratal thinning across a different anticline east of the fault zone (Fig. 7B), from 59 m to 28 m between reflections “6” and “7.”

Additional evidence of distributed off-fault deformation is provided by a prominent submerged shoreline angle and wave-cut platform

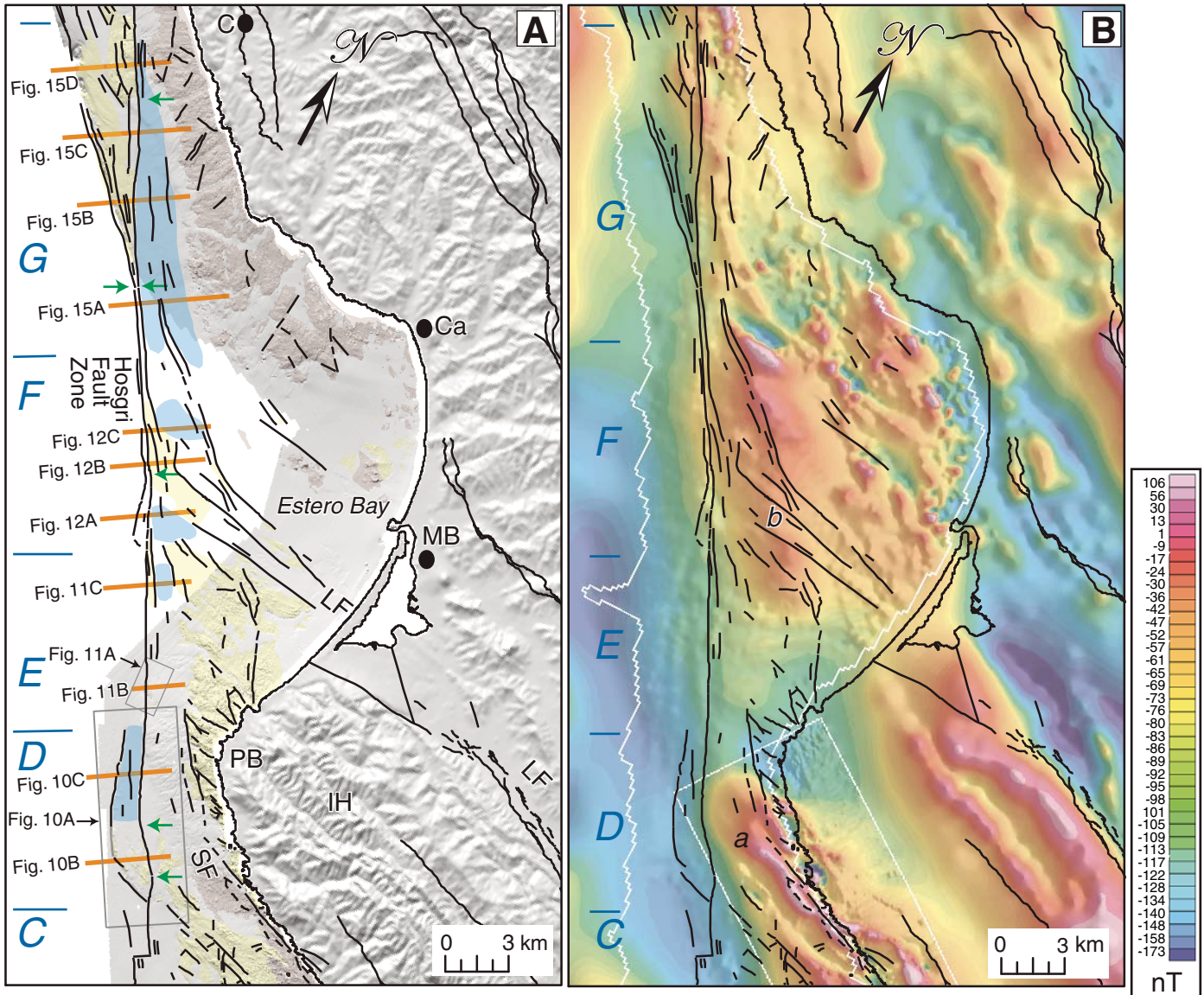
that formed ~1000–2500 m east of section C of the Hosgri fault zone (green triangles on Figs. 7A and 7B). As discussed above, such features record pulses of rapid submergence during the overall post-LGM sea-level rise, providing time/elevation markers for constraining vertical deformation. This shoreline angle extends for ~21 km (into section E) around Point Buchon (Figs. 7 and 9–11), ranging in depth from ~78 m to 91 m. This depth correlates with sea level (~85 m) at ~14 ka during post-LGM Meltwater Pulse 1a (Fig. 3; Peltier, 2005) and the shoreline angle is inferred to have been rapidly submerged (and thus preserved) at that time. Rates of vertical deformation suggested by this feature are discussed in the next section.

#### Section D

Section D of the Hosgri fault extends northwest for 8 km and is distinguished by the presence of a zone of deformation west of the “main Hosgri strand” (“MHS” on Fig. 10) that includes both a leading restraining fault bend and a trailing releasing fault bend (terminology of Mann, 2007). From southeast to northwest, the main Hosgri strand (“MHS” on Fig. 10) trends ~334° in the southern ~1 km of the section, ~320° for the next ~2.5 km, then ~N337° for the northern ~4.5 m of the section. The western deformation zone is initiated at the south end of section D by a west-northwest-trending (290°W) splay.

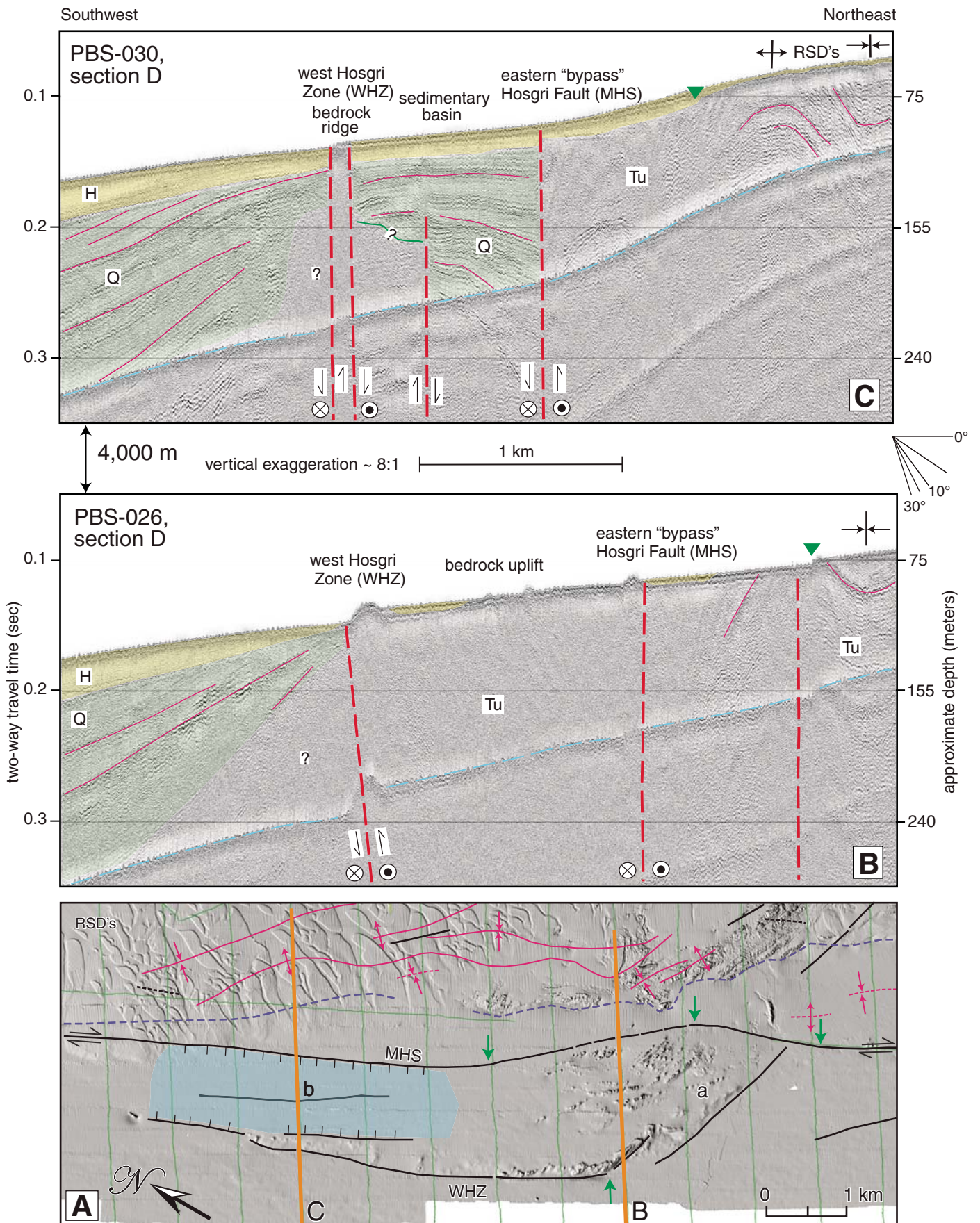
This splay either bends into or is truncated by a “secondary” fault strand(s) (“WHZ”) that lies ~1000–1600 m west of and parallel to (trend ~335°) the MHS. An emergent bedrock uplift (inferred Neogene sedimentary rocks) occupies the southern ~3500 m of the zone between the MHS and WHZ. Bathymetric imagery of the uplift reveals emergent bedrock ribs with discordant trends (Fig. 10A) and the uplift has “reflection free” character on seismic-reflection profiles, consistent with significant internal contractional folding and faulting (Fig. 10B). There is locally as much as 12 m of bathymetric relief (lower to the west) along the WHZ.

In contrast, a relatively undeformed, sedimentary basin occupies the northern ~4000 m of the zone between the MHS and WHZ (Figs. 10A and 10C). The western basin margin is characterized by a narrow (200–400 m wide) fault-bounded bedrock ridge. Basin depth increases to the north and, at the northern end of section D, the WHZ dies out and the basin merges with relatively flat-lying strata of the outer shelf and slope. The presence of the basin and the apparent termination of the WHZ suggest that all lateral fault slip is being transferred back to the eastern MHS in a releasing stepover. Vertical separation on the inferred base of the “H” section along the basin-margin faults is as much as 15 m (Fig. 10C), suggesting local, latest Pleistocene to Holocene vertical offset rates could be as high as 0.75 mm/yr.



**Figure 9.** Central part of study area between Point Buchon (PB) and Cambria (C). Black lines show faults mapped with shallow seismic-reflection data (offshore) and from U.S. Geological Survey (2010) onshore. Blue letters indicate Hosgri fault sections (C, D, E, F, G). (A) Hillshade showing onshore-offshore relief; gray white boundary shows the limit of available multibeam bathymetry. Pale brown and pale yellow polygons show areas underlain by seafloor outcrops of Mesozoic and Neogene bedrock, respectively. Blue-shaded polygons show locations of larger Quaternary basins. Orange bars show locations of seismic-reflection profiles in Figures 10–12, and 15. Green arrows show approximate locations of fault bends. Other abbreviations: Ca—Cayucos; IH—Irish Hills; LF—Los Osos fault zone; MB—Morro Bay; SF—Shoreline fault. (B) Hillshaded magnetic anomaly grid (50 m) based on data in Sliter et al. (2009) and Langenheim et al. (2009). a—northwest-trending magnetic anomaly west of the Shoreline fault. b—magnetic anomalies within Los Osos fault zone east of the Hosgri fault zone. White lines show boundaries of different magnetic surveys. Note that map has been rotated 26° from north.

**Figure 10.** (A) Multibeam (high-resolution bathymetry) image of Hosgri fault section D (see box in Fig. 9) showing bedrock uplift and sedimentary basin (blue shading) associated with paired restraining bend and uplift (a) and releasing stepover and basin (b); locations of seismic profiles PBS-026 and PBS-030 shown in B and C (also see Fig. 9); faults (black lines) with ticks showing downdropping on basin margin; folds (magenta lines); and submerged shoreline angle (purple dashed line). Green arrows show locations of fault bends. Patterned seafloor in upper left results from mobile sand sheets and rippled scour depressions (RSDs; Cacchione et al., 1984). (B) and (C) Interpreted USGS seismic-reflection profiles offshore Point Buchon (Fig. 9). Yellow shading shows latest Pleistocene to Holocene (H) deposits; green shading shows inferred late Quaternary (Q) deposits; Tu—Inferred Neogene bedrock. Red dashed lines show faults; eastern bypass fault is considered the main Hosgri strand (MHS); western fault strand (WHS) splays off the main Hosgri strand and dies out to the north. Thin magenta lines highlight prominent reflections; green triangles show notches in seafloor or subsurface interpreted as a paleo-shoreline angle (e.g., Kern, 1977). Blue dashed line shows seafloor multiple.



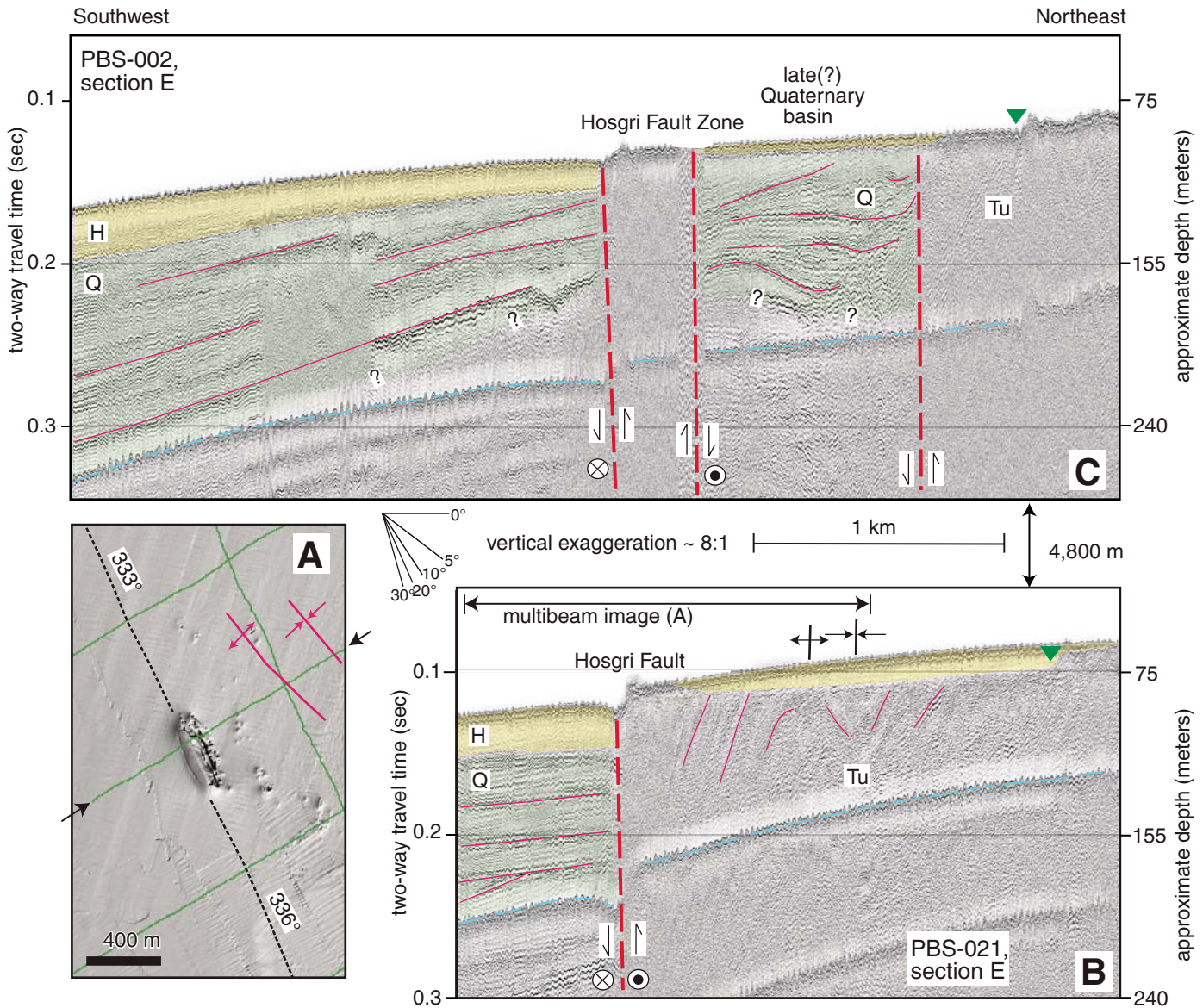


**Figure 11.** (A) Multibeam (high-resolution bathymetry) image of part of Hosgri fault zone section E (see box in Fig. 9) showing 470-m-long bedrock uplift (inferred pressure ridge) and scarp, with arrows showing location of crossing seismic-reflection profile in B. (B) and (C) are interpreted USGS seismic-reflection profiles PBS-021 and 002, offshore Point Buchon (Fig. 9). Yellow shading shows latest Pleistocene to Holocene (H) deposits; green shading shows inferred late Quaternary (Q) deposits; Tu—inferred Neogene bedrock. Red dashed lines show faults; thin magenta lines highlight prominent reflections; green triangles show notches in seafloor or subsurface interpreted as a paleo-shoreline angle (e.g., Kern, 1977). Blue dashed line shows seafloor multiple.

Structurally and in plan view, the geology of section D characterizes the “sidewall ripouts” of Swanson (2005) and the “paired bends” of Mann (2007). Such zones are well documented along strike-slip faults, exist at a variety of scales, and commonly occur in areas of intersecting crustal structure. For section D, the bending occurs within the area where the Hosgri and Shoreline faults converge (Fig. 2), on the western flank of a north-northwest-trending, lobate, magnetic high (“a” on Fig. 9) that we

associate with nearby mapped Jurassic ophiolitic basement (Hall, 1973).

East of section D of the Hosgri fault zone, seismic-reflection and bathymetric data reveal folded and faulted bedrock that is either emergent or buried by a thin sheet of sediment characterized by abundant rippled-scour depressions (Fig. 10A, Cacchione et al., 1984). The well-developed submerged shoreline angle (Fig. 10A) described for section C continues east of the Hosgri fault through section D at

water depths ranging from ~79 m to 90 m. This range provides a datum for estimating the rate ( $\geq \sim 0.4$  mm/yr) of local, post ca. 14 ka vertical deformation (from both faulting and folding) in the zone between the converging Hosgri and Shoreline faults (Figs. 2, 4, and 9).

### Section E

Section E is 8 km long with shallow structure characterized by one or two faults in a relatively

narrow (<500 m) zone (Fig. 11), notably distinct from the paired bend structure and morphology of section D. The section coincides with a relatively low-amplitude, linear, northwest-trending magnetic gradient and lies offshore of the northwest-trending magnetic low associated with the nonmagnetic Neogene sedimentary rocks coring the Pismo syncline (Hall, 1973). Within section E, there is a gentle, gradual left (restraining) bend in fault trend from  $\sim 336^\circ$  in the southern  $\sim 1.5$  km of the section to  $333^\circ$  in the northern part of section E (Fig. 9).

High-resolution bathymetric data, only available for the southern half of this section (Fig. 9A), reveal a prominent, 470-m-long, west-facing scarp that has as much as 18 m of vertical relief (Figs. 11A and 11B) from the crest of the uplift to the base of an elongate trough along the fault trace. Notably, this uplift occurs at the apex of the gradual restraining fault bend where contractional uplift (facilitated by preexisting structural fabric?) is most likely.

Apart from this scarp, bathymetric relief along this section of the fault zone is generally either less than 10 m (e.g., Fig. 11C, typical of the northern  $\sim 3000$  m of section E) or absent. Post-LGM (“H”) strata immediately west of the fault are as thick as 15–20 m (e.g., Figs. 11B and 11C). Together with the bathymetric scarp(s), these data suggest that local, post-LGM vertical offset along the Hosgri fault could be as much as 0.75–1.0 mm/yr.

East of the fault, seismic-reflection profiles (e.g., Fig. 11B) reveal folded Neogene bedrock (Fig. 11A) that is overlain by 0–12 m of post-LGM deposits. On many profiles, this bedrock is reflection free (e.g., Fig. 11C), inferred to result from structural complexity, including relatively steep (< $30^\circ$ ) dips. The prominent, inferred ca. 14 ka shoreline angle described in northern section C and section D occurs in a similar depth range ( $\sim 80$ – $90$  m), again suggesting differential local post-LGM vertical deformation east of the Hosgri fault.

For the northern  $\sim 2.5$  km of section E, the Hosgri fault forms the eastern boundary of a 600- to 1000-m-wide basin (Fig. 11C). Strata within the graben yield parallel to divergent, moderate amplitude, high-frequency reflections, facies considered typical of Quaternary (pre-LGM) deposits. Syndepositional deformation of the basin fill is indicated by internal bidirectional thinning and thickening, and inclined erosional truncations and depositional surfaces.

### Section F

Section F of the Hosgri fault zone extends northwest for 9 km (Fig. 9) and is distinguished (in part) from section E by the presence of sev-

eral closely spaced faults within a broad zone several hundred meters wide (Figs. 9 and 12). The continuous fault that is considered the main Hosgri strand (“MHS” on Fig. 12) gradually bends from an  $\sim 333^\circ$  to  $336^\circ$  trend in the southern  $\sim 3$  km of the section to an  $\sim 327^\circ$  trend in the northern  $\sim 6$  km of the section where it forms the southwest boundary of a basement uplift (Fig. 9). There is no high-resolution bathymetric data for section F and the boundaries of this uplift are based solely on the closely spaced seismic-reflection profiles (Fig. 2).

Section F notably coincides with (1) the convergence of the Hosgri fault zone and a set of west- to northwest-trending, west-diverging faults that we interpret as the offshore extension of the Los Osos fault zone (Lettis and Hall, 1994) (Fig. 9), and (2) truncation of the northwest-trending magnetic high that extends from the north flank of the Irish Hills (Figs. 2 and 9) into the offshore. The southern, west-trending strand of the Los Osos zone appears to die out before reaching the Hosgri fault, while the central and northern strands (and multiple splays) bend to the northwest subparallel to the Hosgri zone. The interaction of these faults with the Hosgri fault appears to control local uplifts and subsidence (Figs. 9 and 12). Most notably, the northern Los Osos strand forms the east boundary of a small ( $\sim 1.5$  km long and wide), shallow (70–90 m deep), synclinal sedimentary basin (Fig. 12C) of inferred late Quaternary age.

Uplifts within the Hosgri fault zone along section F (Figs. 12B and 12C) are typically internally “reflection-free” on seismic profiles, suggesting steep dips, structural complexity, and/or the presence of nonstratified rocks. Bathymetric relief and vertical separation along the Hosgri fault zone varies and can be characterized several ways. On Figure 12B, for example, relief between the peak of the fault-zone uplift and the base of the inferred post-LGM (“H”) section west of the fault is 51 m; the steep bedrock scarp along the main Hosgri strand (MHS) is 10 m high; and the vertical separation between the top of the steep scarp and the base of the post-LGM section west of the fault is  $\sim 26$  m. Because reflections in the post-LGM fill west of the fault appear truncated by the MHS and there is no indication (e.g., seismic facies change) that the contact is a buttress unconformity, the  $\sim 15.5$  m thickness of this fill is considered a minimum estimate for local, post-LGM (ca. 20 ka) vertical offset on the MHS. Minimum, local vertical-offset estimates based on other section F seismic profiles are in the 8–17 m range. Assuming no preexisting scarp relief, rates of vertical deformation along this section of the fault thus fall within a range between  $\sim 0.4$  mm/yr and 0.8 mm/yr

(8–17 m in 20,000 years) and locally could be as high as  $\sim 1.3$  mm/yr (25.5 m in 20,000 years).

As in section D (Fig. 10B), there is a fault “sliver” west of the MHS (Figs. 12A–12C) interpreted as bedrock based on “reflection-free” seismic facies. In contrast to the section D restraining bend uplift, the westernmost section F fault is covered by a thin set of undeformed, continuous, Quaternary (“Q” unit) and post-LGM (“H” unit) reflections. This thin (<50 m) sediment cover suggests that this fault became inactive prior to the LGM in the late Quaternary.

### Section G

Section G of the Hosgri fault zone extends north-northwest for 15 km from northern Estero Bay (Figs. 13 and 14) and is coincident with a linear magnetic gradient. The southern part of this fault section is characterized by two closely spaced ( $\sim 200$ – $250$  m apart) parallel fault strands (Figs. 13 and 15A) that trend  $329^\circ$ , a slightly ( $2^\circ$ ) more northerly bend from the fault trend in the north part of section F. About 2.5 km north of the section F transition, these two fault strands diverge and each strand bends markedly (Figs. 2 and 13). The eastern strand goes through a gradual releasing bend from  $329^\circ$  to  $335^\circ$ , then bends back to a  $329^\circ$  trend in the northern 3–4 km of section G. The western strand goes through a significant restraining bend at the point of fault divergence, from a  $329^\circ$  trend to a  $316^\circ$  trend. The western strand continues this more northwesterly trend for  $\sim 8$  km before it can no longer be mapped in the shallow subsurface,  $\sim 4$  km south of the section G–H transition.

Although high-resolution bathymetric coverage ends slightly east of the western fault strand (Figs. 13 and 14), both multibeam and seismic-reflection data show that the northward-widening wedge between the diverging eastern and western Hosgri strands is an uplifted and beveled ridge consisting of bedrock and possibly folded Quaternary strata that is partly covered by a thin veneer of Holocene sediment (Figs. 14 and 15B). Bedrock is notably emergent in a  $\sim 4$ -km-long by 1-km-wide uplift that occurs along the northern restraining bend on the eastern fault in section G (“a” on Fig. 14).

For much of section G, there is a well-developed lineament and/or east-facing scarp along the trace of the eastern Hosgri fault strand (Fig. 14). The scarp is typically less than 2 m high; however, this increases to as much as 10 m along the noted emergent uplift at the north end of section G.

Vertical separation along the eastern strand, from the top of the bedrock on the west to the base of the inferred post-LGM section on the east varies but commonly falls in the 8–20 m

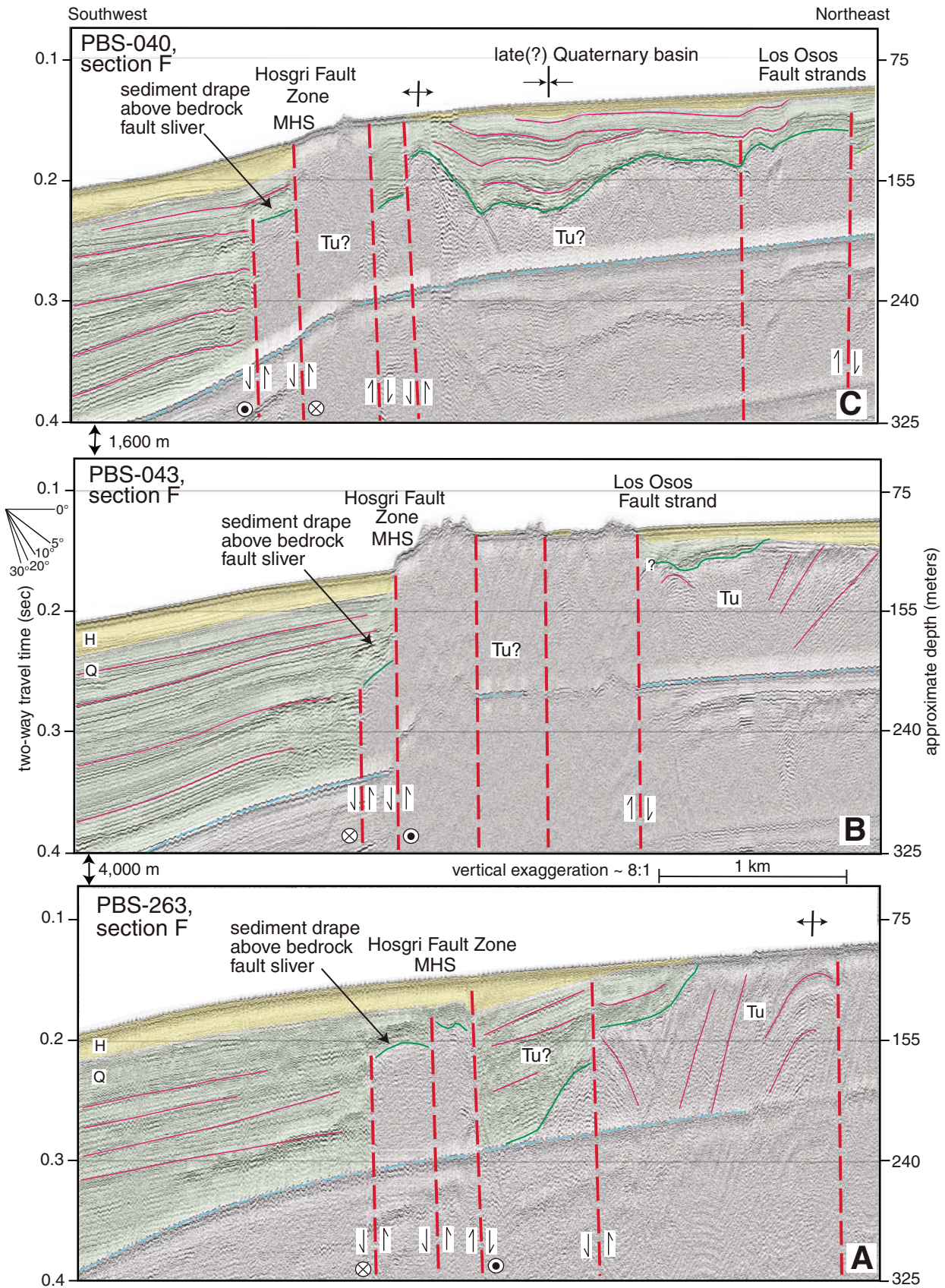
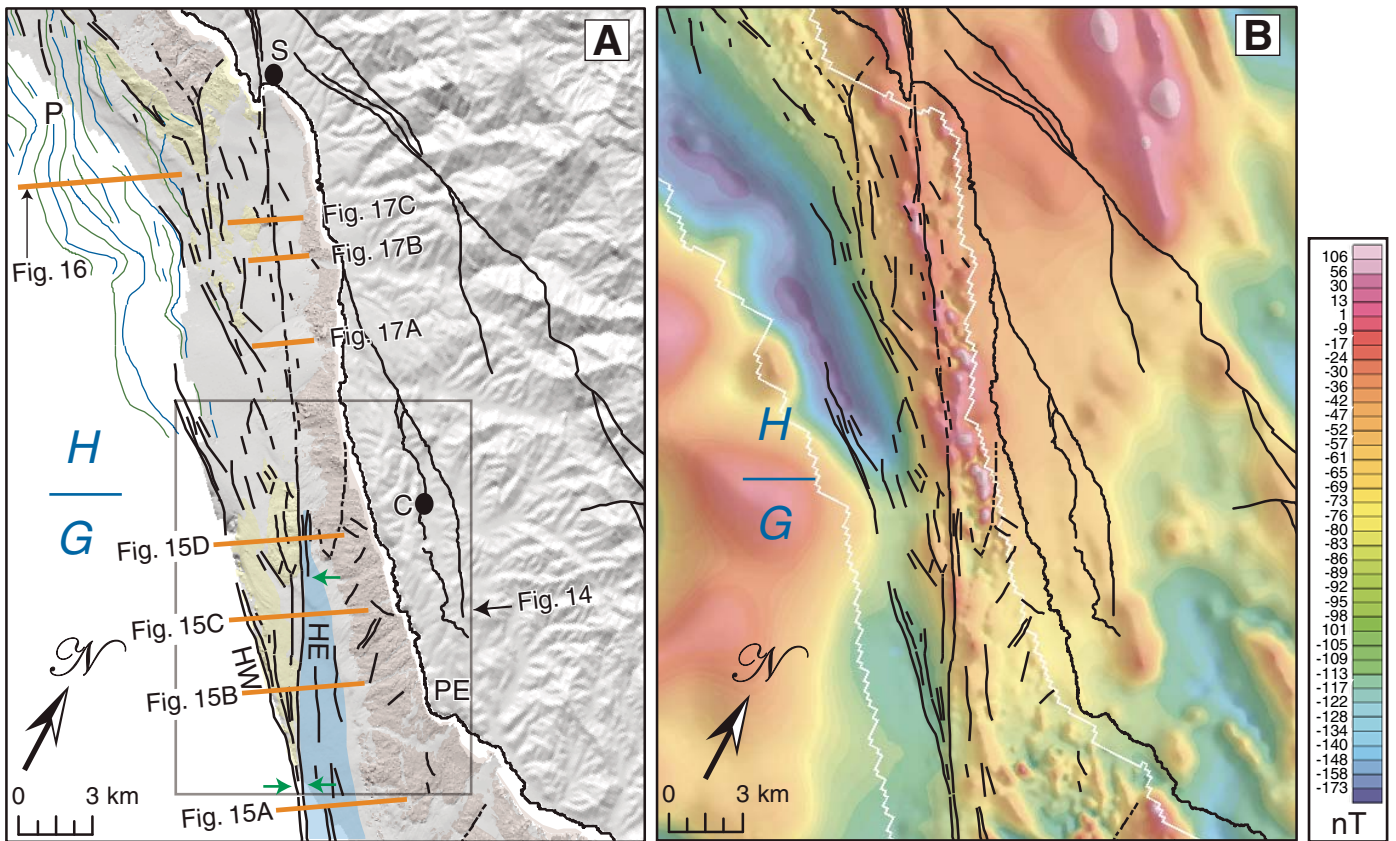


Figure 12. Interpreted USGS seismic-reflection profiles PBS-263 (A), 043 (B), and 040 (C) crossing section F of the Hosgri fault zone, off-shore Morro Bay (Fig. 9). Yellow shading shows latest Pleistocene to Holocene (H) deposits; green shading shows inferred late Quaternary (Q) deposits; Tu?—inferred Neogene bedrock. Red dashed lines show faults; MHS —inferred main strand of Hosgri fault; green lines show unconformity at base of Quaternary section; thin magenta lines highlight prominent reflections. Blue dashed line shows seafloor multiple.



**Figure 13.** Northern part of study area between Point Estero (PE) and San Simeon (S). Black lines show faults mapped with shallow seismic-reflection data (offshore) and from U.S. Geological Survey (2010) onshore. Blue letters indicate Hosgri Fault sections (G, H). (A) Hillshade showing onshore-offshore relief; gray white boundary in the offshore shows limit of available multibeam bathymetry. Pale brown and pale yellow polygons show areas underlain by seafloor outcrops of Mesozoic and Neogene bedrock, respectively. Blue-shaded polygon shows location of Quaternary basin. Green arrows show approximate locations of fault bends. The Hosgri fault zone includes both a west strand (HW) and an east strand (HE). Green and blue lines in the upper left part of map are anticline and syncline axes, respectively, in the Piedras Blancas fold belt (P). Orange bars show locations of seismic-reflection profiles in Figures 15–17. Other abbreviations: C—Cambria. (B) Hillshaded magnetic anomaly grid (50 m). White lines show boundaries of different magnetic surveys. Note that map has been rotated 26° from north.

range. Assuming no pre-LGM relief, the amount of vertical separation suggests variable vertical-offset rates ranging up to 1.0 mm/yr.

The eastern strand of the Hosgri fault zone in section G forms the western margin of an elongate (~15 km) sedimentary basin (Figs. 13–15). The eastern margin of the basin is a west-dipping unconformity over massive (“reflection-free”) Mesozoic bedrock that forms prominent, rugged seafloor outcrops (Fig. 14) continuous with onshore outcrops of Cretaceous sedimentary rocks (Hall and Prior, 1975; Hall et al., 1979). The offshore sedimentary basin narrows from south to north (from ~2400 m to ~300 m wide) and the basin fill is markedly asymmetric (much deeper to the west), thinning northward from more than 200 m to 0 m. This fill is cut by many steep faults that gently warp reflections and have a few meters of dip-slip displacement (Fig. 15).

We infer a late Quaternary age for the basin fill based on relative lack of internal deformation and seismic facies (e.g., reflection frequency, amplitude, and geometry) similar to those of late Pleistocene to Holocene shelf and upper slope deposits on the same seismic profiles.

The elongate nature of the basin and its coincidence with a releasing bend in the Hosgri fault suggest it formed as an immature “Lazy-Z pull-apart basin.” Such basins are common in global strike-slip fault zones; Mann’s (2007, his table 2) compilation lists more than 30 active basins with this inferred origin (including the equivalent “Lazy S” basins of left-lateral fault systems). These basins contrast with rhomboidal pull-apart basins in that they occur along one master fault and are not associated with transfer of fault slip between subparallel overlapping faults.

The northwest-trending western strand of the Hosgri fault zone includes several faults that coincide approximately with the shelfbreak, juxtaposing folded and faulted Neogene bedrock on the east with late Quaternary upper slope deposits on the west (Fig. 15). Vertical separation along the fault (from the top of the bedrock to the base of the inferred post-LGM slope sediment) is difficult to estimate because the slope sediments commonly form an east-thinning wedge that pinches out at the shelfbreak (Fig. 15), but appears to range up to ~10 m.

The bathymetric profile from the outer shelf to the upper slope is typically not smooth (e.g., Figs. 15C and 15D), but rather is characterized by locally concave relief and numerous abrupt slope breaks. The coincidence of some abrupt breaks in slope with faults (Fig. 15C) indicates at least partial tectonic control on shelfbreak/upper

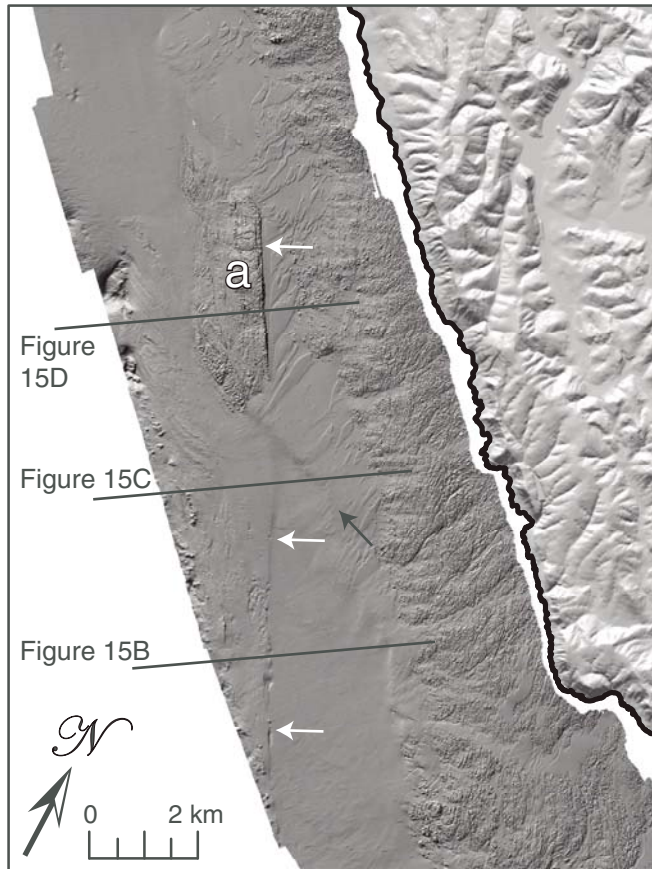


**Figure 14.** Onshore-offshore hillshade digital elevation model (area shown in Fig. 13) with offshore based on multibeam bathymetry. White arrows point to continuous scarp along east strand of gently bending Hosgri fault zone, and a shows large emergent uplift discussed in text. Labeled black lines show locations of the seismic-reflection profiles shown in Figure 15. This fault strand forms the western boundary of a narrow sedimentary basin (see Figs. 9 and 13), bounded on the east by rugged, emergent, seafloor outcrops of Cretaceous sandstone. Note the absence of north-trending scarps or lineaments in these massive, nearshore outcrops. The black arrow shows the base of a low-relief slope. A more detailed multibeam survey will determine if this feature provides a piercing point for determining lateral offset.

slope geomorphology. Submarine landsliding has also been a control, indicated by the presence of abrupt, slope-parallel erosion surfaces (Fig. 15B), multiple slope breaks (Fig. 15C), concave scarp-like features on the upper slope, and probable mass-wasting deposits (e.g., internally massive lenses embedded in well-stratified upper slope deposits, Fig. 15B).

Irregular geomorphology and shallow sediment deformation along the western strand of the Hosgri fault zone clearly indicate recent

faulting, however, significant draping of undeformed sediment above the projection of the fault (e.g., Fig. 15D) also suggests that the western strand dies out or slip is transferred to other structures northward within northern section G and southern section H. The northern termination of the western Hosgri fault zone coincides with the southern margin of a fold belt on the southwest flank of Piedras Blancas (Figs. 13A and 16), the Piedras Blancas anticlinorium of Lettis et al. (2004).

## Section H

Section H is the 328°-trending continuation of the east strand of the Hosgri fault zone as described above in section G. The fault strand extends for 15 km from the north end of the prominent seafloor uplift (Fig. 14) to San Simeon, where it trends onshore and is mapped as the San Simeon fault (Hall et al., 1979; Hanson and Lettis, 1994). The fault is coincident with or parallels linear magnetic gradients interpreted as slivers of Mesozoic mafic rocks. Section H is notable for having a remarkably straight fault trace and the relative absence of obviously young tectonic landforms (e.g., scarps, push-up ridges) or basins adjacent to the fault.

The Hosgri fault zone is not as well imaged on seismic-reflection data in section H (e.g., Fig. 17) compared to sections A–G because of (1) shallow water depth (typically 20–50 m), which increases the amplitude and decreases the depth of the seafloor multiple(s); (2) thin Quaternary sediment cover; and (3) the presence at or near the surface in much of the area of nonreflective (not stratified, steeply dipping, or highly faulted) Mesozoic bedrock (Fig. 13). Given these issues, we increased trackline spacing to 400 m (from 800 m) in the northern 11 km of this section (Fig. 2) and were able to confidently map the Hosgri fault zone based on sharp truncations and/or warping of west-dipping reflections in inferred Neogene strata (Figs. 17B and 17C) and/or clear but small (1–4 m) offset of the base of a post-LGM sediment lens (Fig. 17A).

## DISCUSSION

### Fault Trend and Fault Bends

Offshore investigations combining high-resolution seismic-reflection profiles, bathymetry, and magnetics provide a framework for understanding seafloor tectonic geomorphology and shallow structure along strike-slip faults. Our mapping of the Hosgri fault zone, based on these data, clearly indicates that fault trend is a first-order control on shallow structure, including local uplift and subsidence. The overall trend of the Hosgri over the 94 km between Point Sal and San Simeon is 334.5°, tracing a broad arc from a more northerly general trend in the south (335°–341° in sections A–D) to a more northwesterly trend (328°–334°) in the north (Fig. 2). The Hosgri trend varies locally from as northerly as 340° in section B to as westerly as 320° on the main strand in section D and 316° on the western Hosgri strand in section G. Although there is considerable fault-zone heterogeneity, fault sections or subsections trending ~335°–340° are generally characterized by local basin

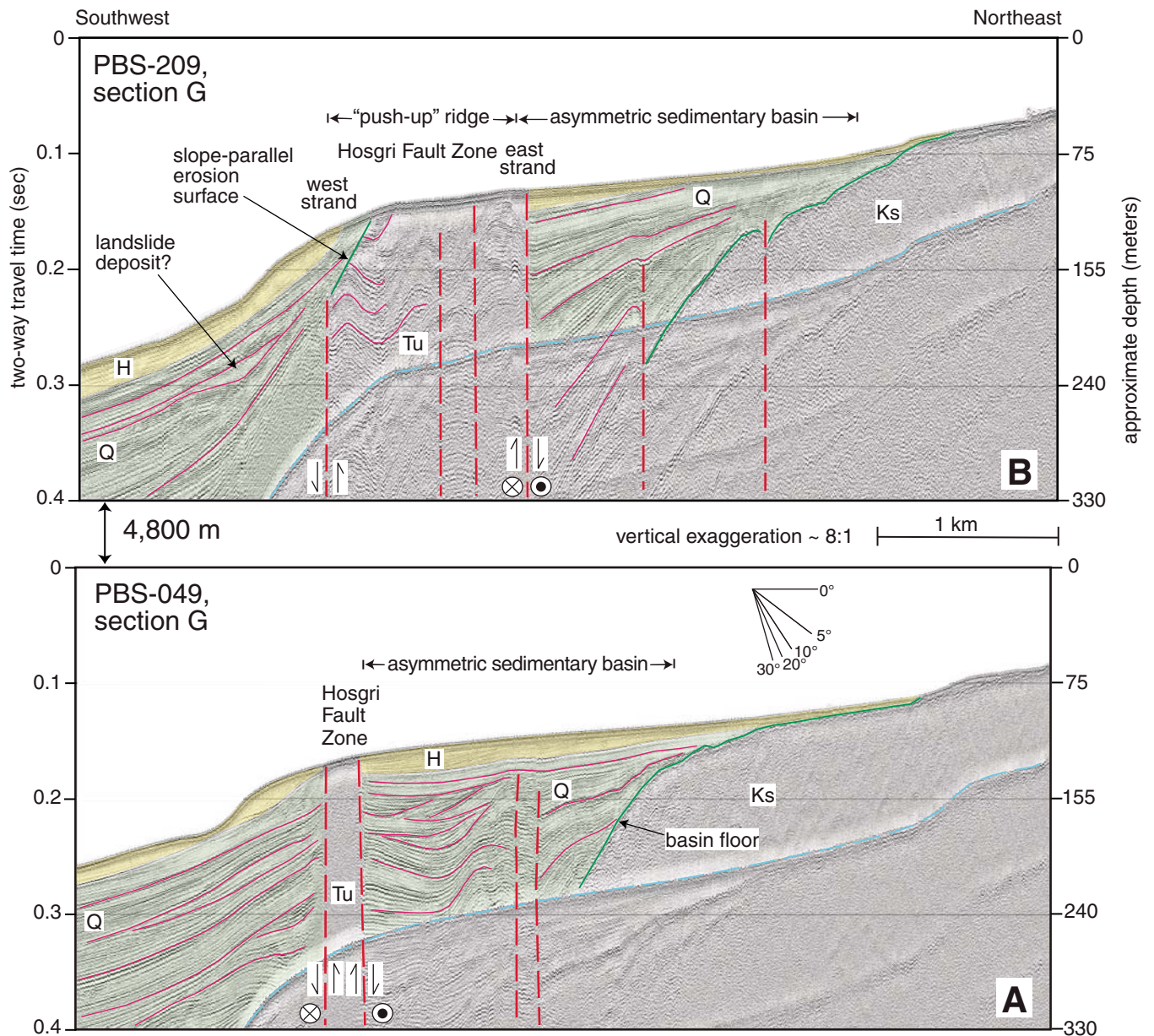


**Figure 15 (Continued on following page).** Interpreted USGS seismic-reflection profiles PBS-049 (A), PBS-209 (B), PBS-230 (C), and PBS-236 (D) crossing section G of the Hosgri fault zone, offshore Cambria (Figs. 2, 13, and 14). Yellow shading shows latest Pleistocene to Holocene (H) deposits; green shading shows inferred late Quaternary (Q) deposits; Tu—inferred Neogene bedrock; Ks—inferred Cretaceous sedimentary rock. Red dashed lines show faults; green lines show unconformity at base of Quaternary section; thin magenta lines highlight prominent reflections; blue triangles on C and D show multiple slope breaks at edge of shelf. Blue dashed line shows seafloor multiple.

formation (subsidence) and transensional deformation, and fault sections and subsections with more westerly trends (<332°) are characterized by transpressional deformation (uplift and folding). A comparison of comparably long (14–15 km) and straight sections B (Fig. 6C) and H (Fig. 17) illustrates this contrast. Faults mapped in section B (trends 340°) cut a thick sequence of undeformed young sed-

iments, whereas section H (trends 328°) cuts uplifted, deformed, and beveled Cretaceous and Tertiary bedrock.

Transitions between transpressional and transensional regimes occur at fault bends that can be gentle and gradual (i.e., a few degrees distributed over a few km) and thus commonly not obvious in map view (Figs. 4, 9, and 13). In section B (fault trend of 339.5°), for example,

the Hosgri is characterized by dip-slip faulting, downwarping, and thick accumulations of Quaternary deposits flanking the fault zone (e.g., Fig. 6C), all indicating subsidence. Gentle warping characterizes the Quaternary section both south (section A) and north (section C) of this zone with the transition zones corresponding to gentle fault bends (e.g., Fig. 6) of 3° and 5°, respectively. Notably, the dilational deformation

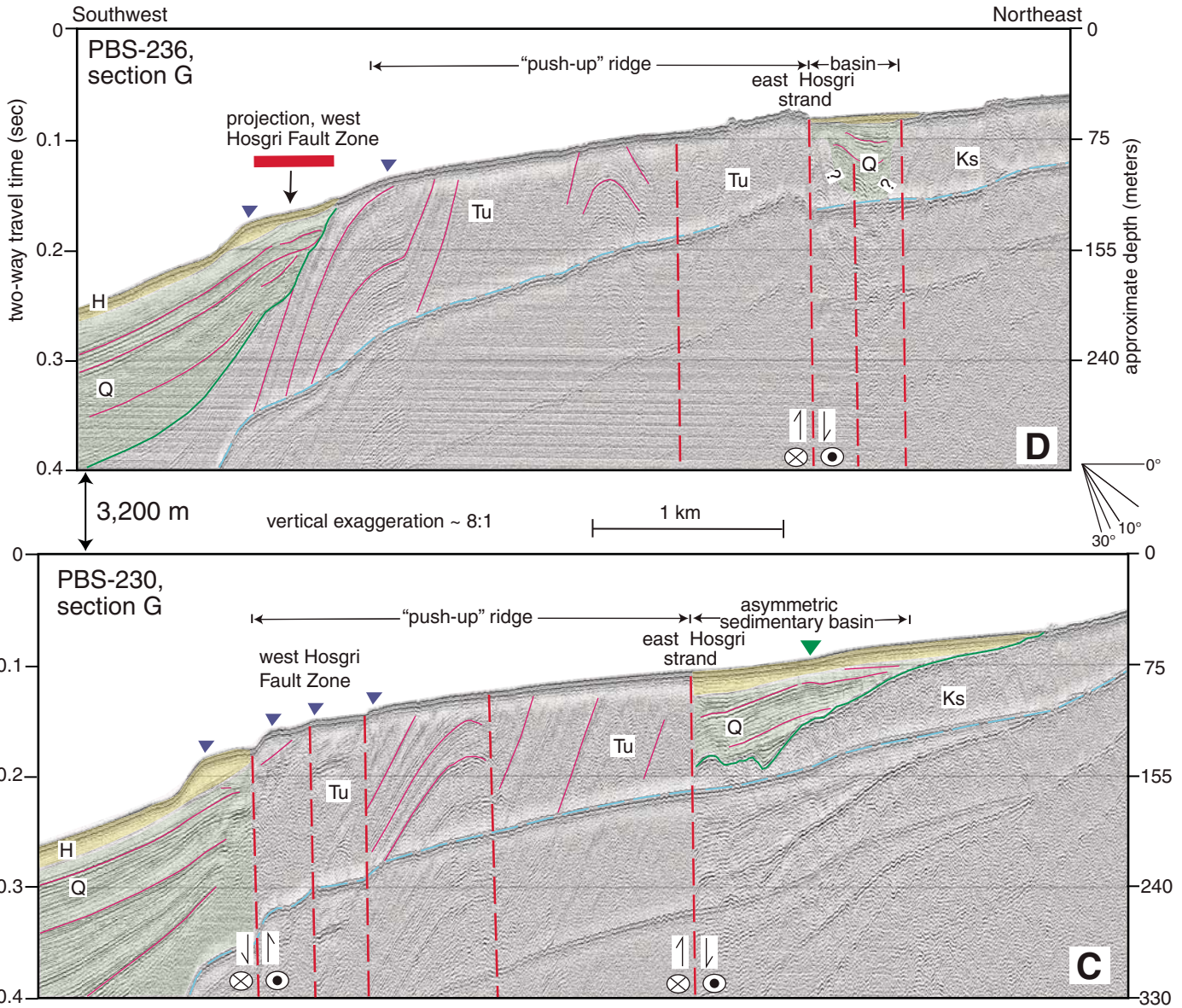


Figure 15 (Continued).

and associated lack of tectonic relief in the fault zone that characterize section B appear to have formed a topographic/bathymetric low, which at least partly controlled the location of the Santa Maria River (at lower sea-level stands) and delta (higher sea levels).

Fault-bounded subsidence associated with transtensional deformation notably occurs in two other sections along the fault associated with similar, more northerly fault trends: (1) The 4.5-km-long stepover basin at the northern end of section D occurs at the trailing edge of a paired restraining-releasing bend (Fig. 10). Basin development is initiated where the Hosgri main strand takes a releasing northerly bend from  $\sim 320^\circ$  to  $\sim 337^\circ$  and slip is transferred

from the western fault strand to the main strand. (2) The 15-km-long “Lazy Z” asymmetric, half-graben occurs along the east flank of the  $335^\circ$ -trending eastern strand of the Hosgri fault zone in section G (Figs. 13 and 14). Basin development is initiated on the south near a  $\sim 6^\circ$  releasing fault bend ( $329^\circ$  to  $335^\circ$ ) and terminates to the north at a gradual  $\sim 7^\circ$  restraining bend ( $335^\circ$  to  $328^\circ$ ). Smaller basins also occur locally within and adjacent to the fault zone (e.g., northern section E, Fig. 11C) where their occurrence appears to be controlled by interactions between the Hosgri fault zone and the converging, northwest-trending, Los Osos and Shoreline faults.

Four fault-zone uplifts with associated contractional deformation are associated with

restraining bends in the Hosgri fault zone and more northwest-trending fault strands:

(1) The uplift at the leading edge of the section D paired restraining-releasing bend occurs where a leading contractional ramp (trends  $\sim 288^\circ$ ) initiates and the trend of the main fault strand changes from  $334^\circ$  to  $320^\circ$  (Fig. 10).

(2) Within Hosgri section E, a 470-m-long, pressure-ridge-like uplift (Figs. 11A and 11B) is associated with a slight  $3^\circ$  northwesterly fault bend ( $336^\circ$  to  $333^\circ$ ).

(3) The uplifted block east of the Hosgri fault zone in section F occurs along a more northwest-trending ( $327^\circ$ ) section of the Hosgri.

(4) A large uplift occurs in section G between the western strand (trends  $316^\circ$ ) and the eastern

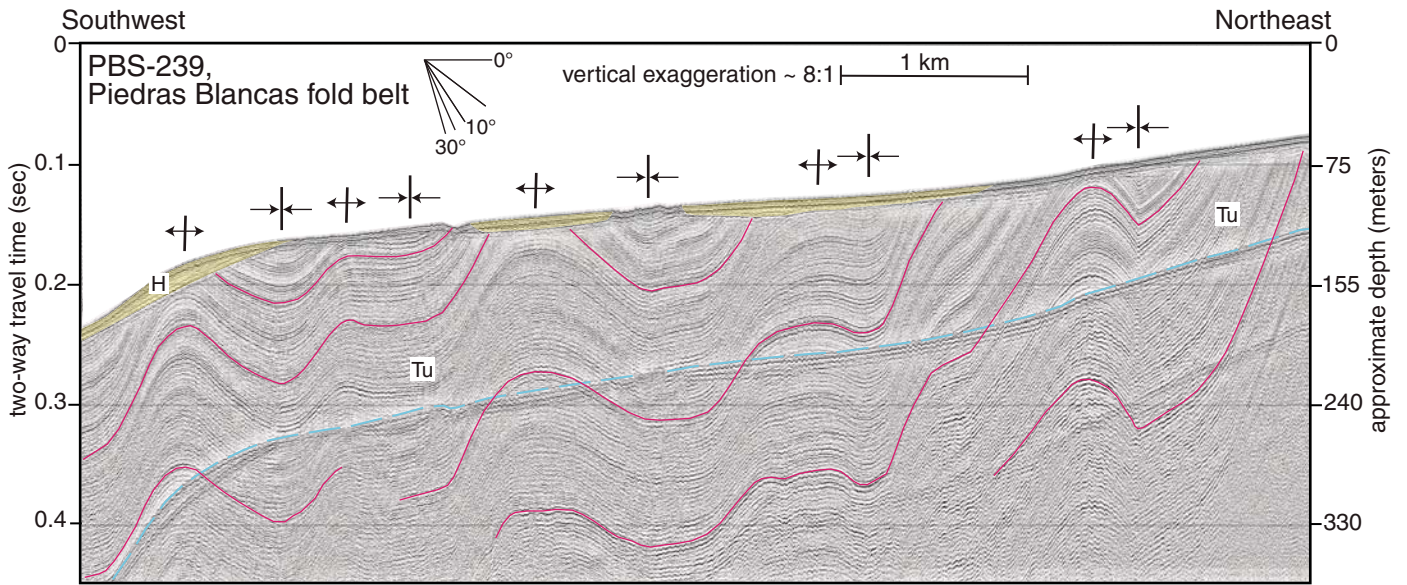


Figure 16. Interpreted USGS seismic-reflection profiles PBS-239 crossing the southern portion of the Piedras Blancas fold belt. Yellow shading shows latest Pleistocene to Holocene (H) deposits; Tu—inferred Neogene bedrock. Thin magenta lines highlight prominent folded reflections. Blue dashed line shows the seafloor multiple.

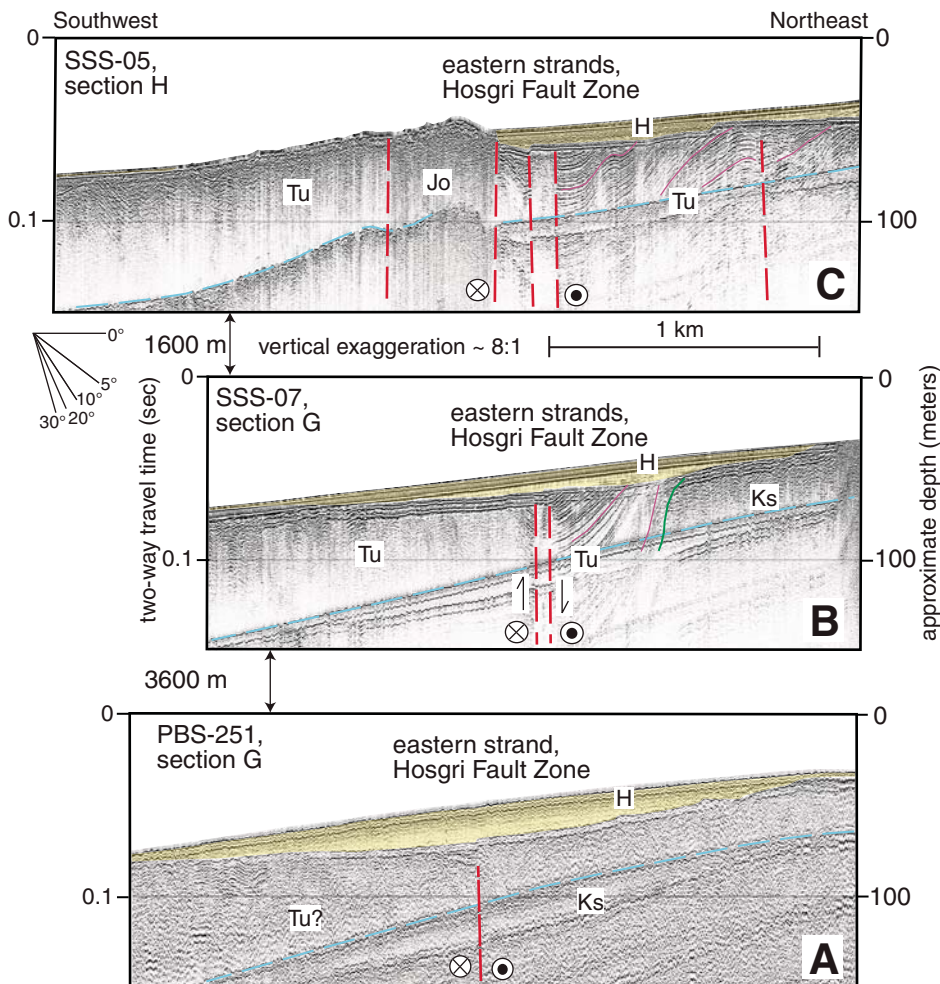


Figure 17. Interpreted USGS seismic-reflection profiles PBS-251 (A), SSS-07 (B), and SSS-05 (C), crossing the Hosgri fault in section H, south of San Simeon. Yellow shading shows latest Pleistocene to Holocene (H) deposits; Tu—inferred Neogene bedrock; Ks—inferred Cretaceous sedimentary rock; Jo—inferred Jurassic ophiolitic rock. Green line on B is inferred unconformity between Cretaceous and Neogene rock. Red dashed lines show faults. Thin magenta lines highlight prominent folded reflections. Blue dashed line shows the seafloor multiple.

strand (trends 335° to 329°) of the Hosgri (Figs. 12–14). The highest seafloor relief (~10 m) in this uplift occurs at the northern boundary of the section G eastern strand along a 6° northwest bend (335° to 329°).

On a larger scale, we also infer that the Piedras Blancas fold belt (Figs. 13, 16, and 18; Lettis et al., 2004) is the result of transpressive fault bending and represents the leading restraining bend uplift of a large paired fault bend (Mann, 2007). We propose that lateral slip is transferred from the western strand of the Hosgri fault zone (section G) to an unmapped oblique-slip blind fault system that forms the southwest and west boundary of the fold belt (leading restraining bend), and lateral slip is transferred back to the Hosgri fault zone north of Piedras Blancas (trailing restraining bend) along the San Martin Structural Discontinuity of McCulloch (1987, his fig. 7) or a similar unmapped structure. Significantly, the fault geometry along the south

flank of Piedras Blancas is nearly identical to that mapped by Ryan et al. (2008, their fig. 1) offshore San Francisco where the San Gregorio fault (Fig. 1, the northern continuation of the Hosgri fault zone) diverges into eastern and western strands, the western strand bends northwest into the oblique-slip Point Reyes fault, and there is significant folding east of and structurally above the Point Reyes fault.

**Fault Convergence**

Our integrated mapping shows that the north-west-trending Lions Head, Casmalia, Shoreline, and Los Osos faults all converge with the Hosgri fault zone from the east within the study area (Figs. 4, 9, and 13). Of these, the latter three converging faults bend abruptly northward within 1 to 2 km of the Hosgri fault zone into near parallelism with the Hosgri before dying out a few km farther to the north-northwest. All of these

convergences are associated with truncation of elongate, fault-parallel magnetic highs, bends in the Hosgri fault zone, recent folding adjacent to the fault, and more complex fault-zone structure. For example, the change in structural style from section A to B (Fig. 6) is attributed to a 4° bend in the fault zone that is forming around an indenting, northwest-trending, magnetic, ophiolitic basement block (“a” on Fig. 4B) that is being translated to the northwest by the Casmalia fault. Future Casmalia fault slip should lead to increasing indentation and development of a transpressive fault bend.

The relationship between the Hosgri and converging faults is more complex where the Shoreline fault converges with section D of the Hosgri fault zone (Fig. 9). At this location, the Shoreline fault forms the northeastern boundary of an elongate magnetic high (“a” on Fig. 9A) that is also inferred to represent a rigid, ophiolitic basement block. This geometry sug-

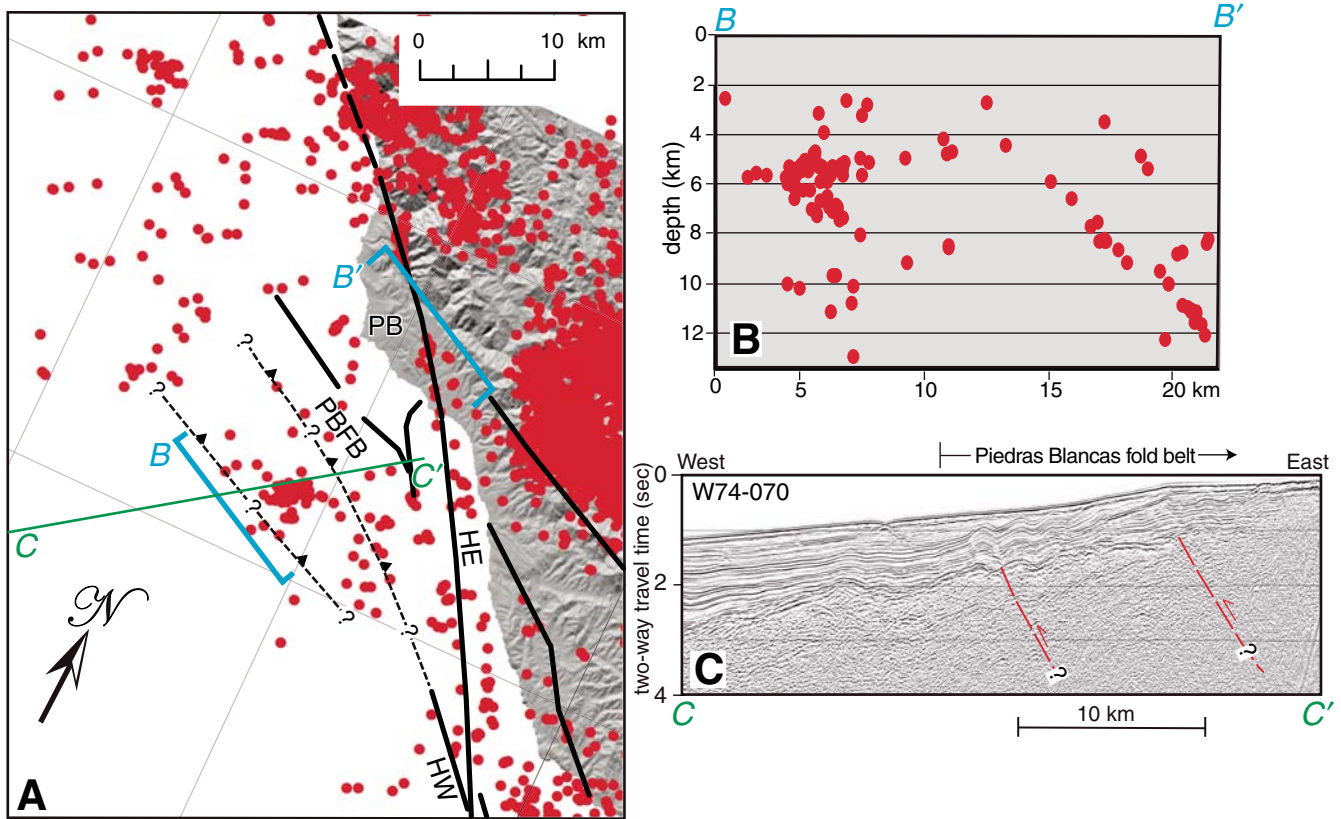


**Figure 18.** Map in (A) showing recorded earthquakes (red dots, database from Hardebeck, 2010) near Piedras Blancas (PB). Black lines show faults. Eastern strand of Hosgri fault (HE) crosses Piedras Blancas onland. Western strand of Hosgri fault (HW) is inferred to bend into a zone of blind oblique thrusting (black dotted lines approximate location of inferred buried fault tips) beneath the offshore Piedras Blancas fold belt (PBFB). Large cluster of earthquakes on east boundary of map is largely associated with the 2003 M 6.5 San Simeon earthquake and its aftershocks (Hardebeck 2010; McLaren et al., 2008; Aron and Hardebeck, 2009). Large cluster of earthquakes in northern onland part of map area is mainly from the 1991 M 5.1 Ragged Point earthquake (McLaren and Savage, 2001). B–B’ shows location of earthquake cross section shown in B. C–C’ shows location of industry seismic-reflection profile W74–070 (U.S. Geological Survey, 2008) shown in C.

gests a four-stage variation of the scenario discussed by Mann (2007, his fig. 12), shown in Figure 19: (1) A rigid magnetic basement block moves along the Shoreline fault so that it abuts and begins to indent the Hosgri fault (as described above for the Casmalia fault). (2) A paired fault bend (“sidewall ripout” of Swanson, 2005) develops around the indenter basement block, characterized by a leading restraining-bend uplift and a trailing releasing-bend basin. (3) A straight bypass fault forms along the original (preindented) trace of the Hosgri fault (main strand), bisecting the indenter basement block as the faults defining the paired bend die out. Bypass, apparently a gradual process, occurs when it becomes more efficient to cut across the indenter block than to bend ever more circuitously around it. (4) The outboard sliver of the bisected indenter basement block subsides on the west flank of the straightened Hosgri fault (main strand) and is translated northward. Geologic and geophysical data (Fig. 10) suggest that the Hosgri-Shoreline fault convergence may now be at the third stage in this scenario,

with both western and bypass strands of the Hosgri fault active. Sims (1993) has discussed similar fault bending and slivering along the San Andreas fault near Parkfield in central California (Fig. 1).

The convergence of the Hosgri fault zone and the Los Osos fault(s) provides further insight on this inferred four-stage (indent-bend-bypass-translate) scenario (Fig. 19). Right-lateral slip on the Los Osos fault zone should be translating the elongate magnetic block that occurs within and on the southwest flank of the zone to the northwest, but it is not obviously indenting section F of the Hosgri fault zone. Where this convergence occurs, the Hosgri fault zone includes several splays and what we interpret as the most tectonic relief in the entire study area. These observations suggest this fault convergence may be at stage 1 in the Figure 19 scenario. Stage 4 is also indicated, however, based on the presence of the buried fault sliver west of the main Hosgri strand (Figs. 9 and 12) that is now being translated northward. It thus seems likely that the inferred four-stage scenario for oblique con-

vergence of strike-slip faults could be repetitive and cyclic, with multiple variations and combinations of stages possible at different sites of fault convergence.

Notably, this model provides a mechanism for generating and translating distinct fault slivers as wide as a few kilometers. It specifically suggests that these slivers form at areas characterized by obliquely converging strike-slip faults (Fig. 20) and can be generated more than once in the history of such convergence. This increases the probability of occurrence of multiple piercing points with different amounts of offset along the Hosgri and other strike-slip fault zones. In central California, it provides a potential explanation for the extremely variable estimates of cumulative dextral offset (5–180 km) on the Hosgri-San Gregorio fault system (summarized in Hanson et al., 2004; Dickinson et al., 2005; Burnham, 2009).

#### Local, Short-term Vertical Deformation

The Hosgri fault zone forms the eastern margin of the deep, offshore Santa Maria basin (e.g., McCulloch, 1987); hence long-term vertical slip on the Hosgri is clearly down to the

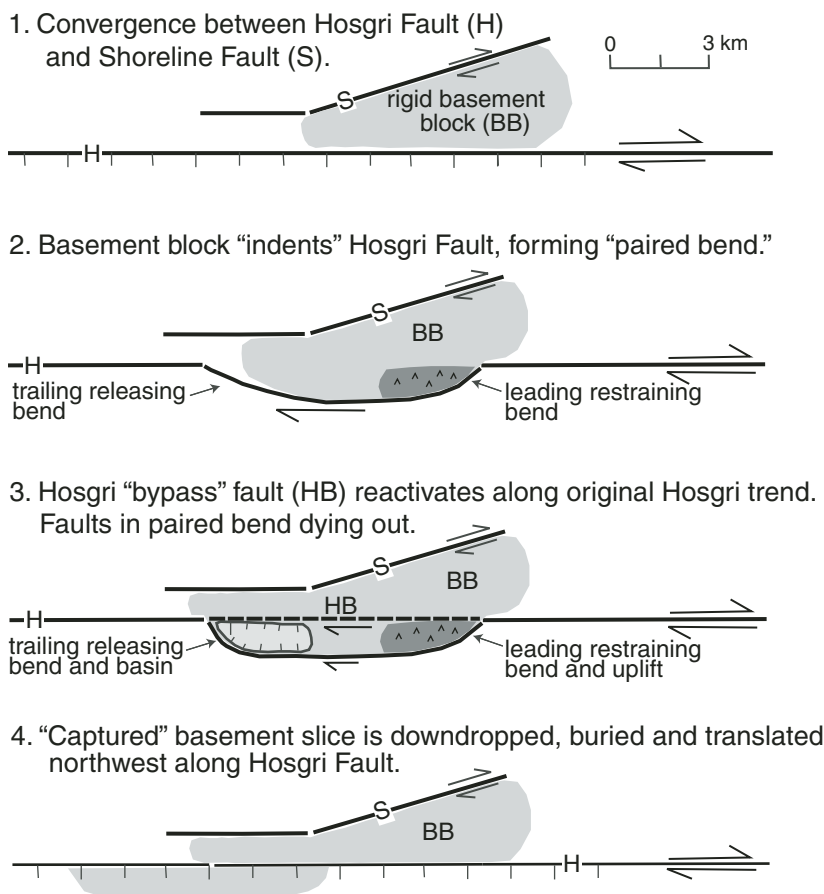


Figure 19. Schematic model for generation of paired fault bend (follows Mann, 2007) adopted for zone of convergence between Hosgri and Shoreline faults. See text for discussion.

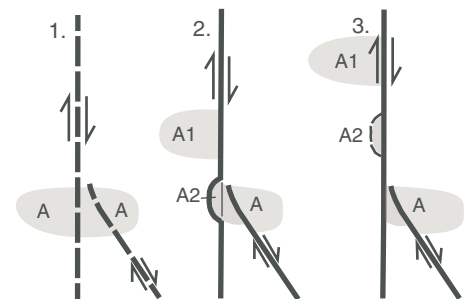


Figure 20. Hypothetical scenario in which a distinctive rock unit (A) could yield multiple piercing points and different estimates of fault offset along a strike-slip fault. In step 1, tectonic reorganization leads to initiation of a north-trending master strike-slip fault and a converging, northwest-trending strike-slip fault. In step 2, offset along the master fault has translated block A1 away from its source, and offset on the northwest-trending fault has resulted in indentation and bulging of the master fault, creating a paired bend (see Fig. 19). In Step 3, the master fault has broken through the Step 2 bulge and a second block of unit A (A2) is translated northward. The result is two different offset blocks of unit A that could yield two different piercing points and estimates of cumulative offset along the master strike-slip fault.

west. Hanson et al. (2004; see their table 3 and fig. 17) interpreted a large database of deeper penetration, lower-resolution, seismic-reflection profiles to document the west-side-down vertical slip rates on the Hosgri fault zone between Point Arguello and Morro Bay (Fig. 1), an area that includes sections A–F of this study. Their comprehensive study used a top-of-Miocene (ca. 5.1 Ma) unconformity and an early-late Pliocene unconformity (ca. 2.8 Ma) as stratigraphic markers to obtain variable, down-to-the-west, long-term vertical slip rates that typically fall in the range of 0.1–0.4 mm/yr. Our study adds to this work but differs significantly in that we mainly use the post-LGM unconformity (ca. 20 ka) and young geomorphic surfaces (e.g., scarps, submerged shoreline angles) to estimate local, short-term vertical deformation rates. Because relief in strike-fault zones can evolve rapidly and tectonic inversion is common (e.g., Christie-Blick and Biddle, 1985; Yoshioka, 1996; Barnes et al., 2001), these shorter term rates provide more insight into active tectonics and seafloor geomorphology but less information on longer term vertical slip rates and evolution of the Hosgri fault system.

Seismic-reflection profiles reveal evidence of both west-side-down (e.g., Figs. 4, 10B, 10C, 11B, and 12A–12C) and east-side-down vertical displacement (e.g., Figs. 7B, 15C, 15D, 17C, and 17D) and some profiles image push-up ridges within the fault zone with downward vertical separation on both flanks (e.g., Figs. 6B, 10C, 11C, 15A, and 15B). Estimated rates of vertical offset on different seismic profiles range from 0 to as much as 1.4 mm/yr (Fig. 12B), but are generally less than ~0.7 mm/yr. These rates are highly variable over short distances (i.e., between 800 m seismic-reflection profiles), and are clearly locally controlled by fault trend, fault bends, and fault convergences (see above).

Several seismic-reflection profiles also image fold growth and shortening east of the Hosgri fault zone, most prominently in areas where the Hosgri converges with the Shoreline, Los Osos, and Casmalia faults (Fig. 2). Variable elevations of the submerged Pleistocene shoreline angle (see above and Figs. 3, 7, 10, and 11; correlated with ca. 14 ka Meltwater Pulse 1A) that occur within 1 km of the Hosgri fault zone suggest vertical deformation rates (from folds and faults) as much as 0.4 mm/yr or more. These inferred rates are notably higher than nearby onland uplift rates (0.2 mm/yr) based on detailed analyses of marine terraces (Hanson et al., 1994). The overall pattern indicates that vertical deformation is highest within and in proximity (~1–2 km) to the Hosgri fault zone, especially where the Hosgri converges with the Shoreline and Los Osos faults, and diminishes to the east and west.

## EARTHQUAKE HAZARD IMPLICATIONS

Earthquake hazard assessments (e.g., Petersen et al., 2008) depend on characterization of earthquake source zones (i.e., faults), including documentation of fault location and length, fault geometry (dip), and sense of slip, slip rate, and earthquake history and recurrence. This paper provides new information on several of these source parameters for the Hosgri fault zone.

### Fault Location and Length

Our detailed mapping of the Hosgri fault zone (Figs. 2, 4, 9, and 13) from offshore Point Sal north to offshore Point Estero shows the Hosgri fault zone in the approximate location as previous studies (e.g., McCulloch, 1987; Pacific Gas and Electric Company, 1988; Lettis et al., 2004). Farther north, between Point Estero and San Simeon, our new data resolve a fault-mapping conflict.

Previous interpretation of the Hosgri fault zone have suggested that it ends a few km north of Point Estero (e.g., Pacific Gas and Electric Company, 1988) and slip is transferred as much as 5 km to the east on to the subparallel offshore portion of the dextral San Simeon fault. The San Simeon fault is described as an inferred, discrete structure that extends parallel to the coast (~400–1400 m offshore) for ~27 km from Point Estero to landfall at San Simeon. Where the faults overlap, the transfer of slip (i.e., stepover) results in the development of a rhomboidal pull-apart basin (DiSilvestro et al., 1990; Lettis et al., 1990; Hanson et al., 2004). The width of the stepover (~5 km) is considered too large for a transfer of slip during a large earthquake, so the maximum rupture length for an earthquake along the Hosgri fault zone is the distance between a Hosgri endpoint northwest of Point Estero and the southern termination of the fault offshore Point Arguello (Steritz and Luyendyk, 1994; Lettis et al., 2004), ~110 km.

The above interpretation was made without the benefit of the comprehensive seismic reflection, magnetic, and bathymetric database used in this study. Our mapping based on the new data shows that the offshore eastern strand of the Hosgri fault is continuous with the mapped onshore San Simeon fault (e.g., Figs. 1, 2, and 13; Leslie, 1981), which is continuous and well mapped onshore at Piedras Blancas (Hall, 1976; Hall et al., 1979). We find no evidence of the inferred offshore San Simeon fault between San Simeon and Point Estero (Figs. 13 and 14) and consider the absence of a bathymetric scarp or lineament on the shallow bedrock

shelf that underlies this part of the coast, in contrast to the lengthy scarp along the Hosgri fault farther offshore, an especially compelling observation. As described above (section G), we interpret the inferred 3- to 5-km-wide pull-apart basin, a key component of the stepover interpretation, as a narrower (width <2400 m), immature “Lazy Z basin.”

Hence, detailed mapping of the Hosgri-San Simeon fault system indicates a continuous fault zone from Point Sal to the north flank of Piedras Blancas, and we consider this distance, ~110 km, a minimum rupture length. Longer ruptures are certainly possible (e.g., Petersen et al., 2008) but these estimates are not supported by similar comprehensive offshore mapping efforts, either south of Point Sal or (especially) north of Piedras Blancas (Fig. 1).

### Fault Geometry and Sense of Slip

Hanson et al. (2004; their table 1) used diverse data including deep and shallow seismic-reflection profiles, seismicity, and regional geology to present a very strong case that the Hosgri fault is a steep, right-lateral, strike-slip fault zone. Our new data and mapping strongly support that interpretation, specifically noting: (1) The Hosgri fault is a long, linear zone of faulting. (2) Faults in the Hosgri zone in the shallow subsurface are steep (dip ~70° to 90°). (3) The Hosgri fault zone is characterized by a mix of extensional and contractional deformation. (4) Patterns of uplift and subsidence along the fault conform to predicted patterns for fault bends and stepovers in a right-lateral system. (5) There are large changes in the style, rate, and symmetry of vertical deformation along the fault zone.

### Lateral Fault Slip Rates

Regional geodetic modeling of fault systems in central California suggests that the Hosgri has a right-lateral slip rate of ~4 mm/yr (McCaffrey, 2005; Meade and Hager, 2005). Hanson and Lettis (1994) suggested slip rates of 1–3 mm/yr for the Hosgri-San Simeon fault system based on geologic data (offset marine terrace strandlines and drainages) at San Simeon (Figs. 1 and 13). Our survey produced no new direct information on lateral slip rates (e.g., dated piercing points); however, our analysis does suggest that slip is partitioned between two Hosgri fault strands in the northern part of the area and hence the suggested slip rates from the onshore San Simeon work should be regarded as only a minimum estimate.

As described above, the Hosgri fault zone bifurcates in section G into two main strands.

The eastern strand is continuous with the onshore San Simeon fault, whereas the western strand appears to end north of the bifurcation and transfer slip to other structures (Figs. 13, 15, and 18). Termination of the western strand coincides with the onset of folding in the Piedras Blancas fold belt and we infer that these two phenomena are linked—that fault slip is being partly transformed into strain (permanent deformation) within the fold belt. If slip from the western Hosgri strand were instead transferred back to the eastern strand, there should be an extensional stepover in the area where the faults overlap instead of the noted bedrock uplift (Figs. 13–15). Thus, there is a loss of slip northward along the Hosgri system and estimates of fault slip at San Simeon account for only part of the fault slip south of section G. Because we lack information on the timing and rate of deformation in the Piedras Blancas fold belt, we have no solid estimate for the amount of lost slip.

Previously, Hanson et al. (2004, their fig. 18) suggested that slip along the Hosgri Fault decreases southward (by  $\sim 0.4$  mm/yr) from the 1–3 mm/yr at San Simeon to Point Sal, as slip is consumed by crustal shortening east of the Hosgri fault along more westerly trending faults (e.g., Los Osos fault, Casmalia fault) within the Los Osos domain (Fig. 1). Given inferences for loss of slip both to the north and to the south along the Hosgri fault zone, it seems clear that lateral slip rates along the Hosgri system are both complex and variable. However, given that (a) geodetic estimates of lateral slip on the Hosgri are 3–4 mm/yr, and (b) geology-based estimates of 1–3 mm/yr at San Simeon can be considered minimum Hosgri rates, we think it is likely that Hosgri lateral slip rates in this area fall within the range of 2–4 mm/yr.

### Earthquake Recurrence and History

Information on earthquake recurrence and history is integral to time-dependent, probabilistic seismic hazard assessment (Petersen et al., 2007) but is lacking for the Hosgri fault zone. From onland studies near San Simeon, Hall et al. (1994) estimated earthquake recurrence falls within the range of 265–2000 yr for one strand of the Hosgri fault (1–2 m slip events), but this work is considered preliminary, based on several assumptions (e.g., strike slip:dip slip ratio of 8:1–10:1), and there is no direct information on earthquake history. It may be that offshore, intrafault zone basins contain a stratigraphic record of large earthquakes as has been shown by McHugh et al. (2006) in intrafault zone basins along the North Anatolian fault in Marmara Sea. Strong earthquakes may have also triggered shelfbreak landslides (e.g., Fig. 15)

and landslide deposits may also contain a partial paleoseismic record. In these scenarios, strong ground motions would cause slope failures or otherwise mobilize coarser sandy sediment and transport it to depositional sites in basins or along scarps that are dominated by background, mud-dominated deposition. Seismic-reflection profiling reveals several potential intrabasinal (e.g., Figs. 10, 11, and 15) and along-scarp sites (e.g., Figs. 10–12 and 15) where this hypothesis could be tested.

### OTHER POTENTIAL EARTHQUAKE SOURCES

#### Constraints on Shoreline Fault Offset

Hardebeck (2010) recognized the Shoreline fault based on an  $\sim 25$ -km-long linear trend of micro-seismicity just offshore and parallel to the coast along the southwest flank of Point Buchon (Figs. 2, 4, and 9). The structure has been mapped at the surface based largely on discontinuous bathymetric and magnetic lineaments (Langenheim et al., 2012); seismic-reflection data have been less effective due to shallow water and the predominance of massive, “reflection-free,” structurally deformed bedrock with minimal sediment cover. Information on fault offset is lacking. Above, we propose a scenario (Fig. 19) in which offset on the Shoreline fault resulted in indentation, bulge, and development of a paired restraining and releasing bend in the Hosgri fault zone. If (1) this scenario is valid, and (2) the width of the Hosgri bulge corresponds to the amount of indentation and thus approximates the amount of lateral fault slip, then there has been a minimum of  $\sim 1.4$  km of lateral slip on the Shoreline fault.

#### Is the Piedras Blancas Fold Belt an Earthquake Source?

We propose a hypothesis in which bending of the western strand of the Hosgri fault zone has led to shortening and transpressive uplift of the Piedras Blancas fold belt above an unmapped blind fault zone that could involve oblique and/or thrust offset (Fig. 18). No similar fold belt is known elsewhere west of the Hosgri fault and its location coincident with the northward end of the western Hosgri strand in section G (Fig. 13) suggests that these two phenomena are linked, that slip on the western strand is accommodated by Piedras Blancas folding and blind oblique thrust faulting. If correct, then determining the timing and rate of fold belt deformation is important for understanding both slip distribution along the Hosgri fault and the Piedras Blancas fold belt as an independent earthquake source.

The shelf offshore Piedras Blancas is mostly underlain by folded Neogene rocks (Fig. 16) that are typically beveled and often overlain by a thin, discontinuous cover (typically less than 5–10 m) of post-LGM sediment. Line-length analysis of the folded bedrock using deeper industry seismic-reflection data (Fig. 18C) indicates fold-belt shortening of about 4%. Deformation must postdate deposition of the middle to late Miocene Monterey Formation (younger than ca. 7 Ma), which is involved in the folding but does not reveal significant stratal thinning or thickening (i.e., no evidence of growth folding) on high-resolution seismic-reflection data (e.g., Fig. 16). Given the setting, Quaternary and active folding seems likely but cannot be proven from our seismic-reflection data because post-LGM sediment cover is too young and too thin and older Quaternary deposits are largely missing. Seismicity (Figs. 18A and 18B) provides some evidence of active deformation in the Piedras Blancas fold belt and is consistent with our proposed hypothesis. McLaren and Savage (2001) and Hardebeck (2010) report a mix of thrust and strike-slip earthquakes in this offshore region, and several events align on northeast-dipping ( $\sim 45^\circ$ ) planes beneath the fold belt.

We think the existing seismotectonic data support recognition of the Piedras Blancas fold belt as an independent earthquake source. We anticipate that future earthquake monitoring and targeted offshore geophysical studies will provide better constraints on the earthquake hazard associated with this source.

### CONCLUSIONS

Comprehensive geophysical data are used to map the strike-slip Hosgri fault zone offshore central California. Mapping documents the location, length, and near-surface continuity of multiple fault strands, highlights fault-zone heterogeneity, and demonstrates the importance of fault trend, fault bends, and fault convergences in the development of shallow structure and tectonic geomorphology.

The dextral Hosgri fault zone is continuous in the offshore for  $\sim 94$  km from Point Sal to Piedras Blancas, passing through a broad arc in which fault trend changes south to north from  $\sim 338^\circ$  to  $328^\circ$ . The southern  $\sim 40$  km of the fault zone in this area is more extensional, resulting in accommodation space that is filled by deltaic sediments of the Santa Maria River. The central  $\sim 24$  km of the fault zone is characterized by oblique convergence of the Hosgri fault zone with the more northwest-trending Los Osos and Shoreline faults. Convergence between these faults has resulted in the formation of local

restraining and releasing fault bends, transpressive uplifts, and transtensional basins of varying size and morphology. We present a hypothesis that links development of a paired fault bend to indenting and bulging of the Hosgri fault by a strong crustal block translated to the northwest along the Shoreline fault.

Two diverging Hosgri fault strands bounding a central uplifted block characterize the northern ~30 km of the Hosgri fault in this area. The eastern Hosgri strand passes through releasing and restraining bends; the releasing bend is the primary control on development of an elongate, asymmetric, "Lazy Z" sedimentary basin. The western strand of the Hosgri fault passes through a significant restraining bend and dies out northward where we propose that its slip transfers to active blind structures in the Piedras Blancas fold belt.

Given the continuity of the Hosgri fault zone through our study area, earthquake hazard assessments should incorporate a minimum rupture length of 110 km. Our data do not constrain lateral slip rates on the Hosgri, which probably vary along the fault (both to the north and south) as different structures converge and diverge but are likely in the geodetically estimated range of 2–4 mm/yr. The post-Last Glacial Maximum (LGM) unconformity is an important surface for constraining vertical deformation, yielding local vertical deformation rates that may be as high as 1.3 mm/yr and off-fault deformation rates as high as 0.5 mm/yr. These local vertical rates are short-term and not sustainable over longer geologic time, emphasizing the complex evolution and dynamics of strike-slip zones.

#### ACKNOWLEDGMENTS

This work was jointly funded by the USGS Coastal and Marine Geology Program, National Geologic Mapping Program, and Pacific Gas and Electric Company (PG&E) through a Collaborative Research and Development Agreement. We thank Roberto Anima, Jeff Beeson, Mike Boyle, Mark Kocina, Jackson Currie, Jamie Grover, Pat Hart, Gerald Hatcher, Larry Kooker, Daniel Scheirer, Ray Sliter, George Tate, Peter Triezenberg, and Robert Wyland for assistance in collection of USGS seismic-reflection and marine magnetic data. We are grateful to the California Ocean Protection Council for supporting the California Seafloor Mapping Program and high-resolution bathymetric mapping with special thanks to Sheila Semans. We thank Rikk Kvitek and the California State University at Monterey Bay Seafloor Mapping Lab for completing the bathymetric mapping and continuing strong collaboration. We have benefitted from stimulating discussions with Hans Abramson, Jeff Beeson, Tim Dawson, Bill Ellsworth, Russ Graymer, Gary Greene, Katherine Hanson, Steve Hartwell, Vicki Langenheim, Bill Lettis, Stu Nishenko, Bill Page, Tom Parsons, Holly Ryan, Gordon Seitz, Ray Sliter, Steve Thompson, Carl Wentworth, and Chris Wills. Holly Ryan, Gary Greene, and Paul Mann provided stimulating and constructive reviews.

#### REFERENCES CITED

- Anima, R.J., Eittreim, S.L., Edwards, B.D., and Stevenson, A.J., 2002, Nearshore morphology and late Quaternary geologic framework of the northern Monterey Bay Marine Sanctuary: *Marine Geology*, v. 181, p. 35–54, doi:10.1016/S0025-3227(01)00260-2.
- Argus, D.F., and Gordon, R.G., 2001, Present tectonic motion across the Coast Ranges and San Andreas fault system in central California: *Geological Society of America Bulletin*, v. 113, p. 1580–1592, doi:10.1130/0016-7606(2001)113<1580:PTMATC>2.0.CO;2.
- Aron, A., and Hardebeck, J.L., 2009, Seismicity rate changes along the central California coast due to stress changes from the 2003 M 6.5 San Simeon and 2004 M 6.0 Parkfield earthquakes: *Bulletin of the Seismological Society of America*, v. 99, p. 2280–2292, doi:10.1785/0120080239.
- Arrowsmith, J.R., and Zielke, O., 2009, Tectonic geomorphology of the San Andreas Fault Zone from high-resolution topography—An example from the Cholame segment: *Geomorphology*, v. 113, p. 70–81, doi:10.1016/j.geomorph.2009.01.002.
- Ballance, P.F., and Reading, H.G., 1980, Sedimentation in Oblique-slip mobile zones: *International Association of Sedimentologists Special Publication* 4, 265 p.
- Barnes, P.M., Sutherland, R., Davy, B., and Deltiel, J., 2001, Rapid creation and destruction of sedimentary basins on mature strike-slip faults: An example from the offshore Alpine Fault, New Zealand: *Journal of Structural Geology*, v. 23, p. 1727–1739, doi:10.1016/S0191-8141(01)00044-X.
- Biddle, K.T., and Christie-Blick, N., eds., 1985, Strike-slip deformation, basin formation, and sedimentation: *Society of Economic Paleontologists and Mineralogists Special Publication* 37, 385 p.
- Briggs, I.C., 1974, Machine contouring using minimum curvature: *Geophysics*, v. 39, p. 39–48.
- Bruns, T.R., Cooper, A.K., Carlson, P.R., and McCulloch, D.S., 2002, Structure of the submerged San Andreas and San Gregorio Fault zones in the Gulf of Farallones as inferred from high-resolution seismic-reflection data, in Parsons, T., ed., *Crustal structure of the coastal and marine San Francisco Bay region*, California: U.S. Geological Survey Professional Paper 1658, p. 77–117.
- Burnham, K., 2009, Predictive model of San Andreas Fault system paleogeography, Late Cretaceous to early Miocene, derived from detailed multidisciplinary conglomerate correlations: *Tectonophysics*, v. 464, p. 195–258, doi:10.1016/j.tecto.2007.11.056.
- Cacchione, D.A., Drake, D.E., Grant, W.D., and Tate, G.B., 1984, Rippled scour depressions of the inner continental shelf off central California: *Journal of Sedimentary Petrology*, v. 54, p. 1280–1291.
- California State University Monterey Bay Sea Floor Mapping Lab, 2010: [http://seafloor.csumb.edu/SFMLwebDATA\\_c.htm](http://seafloor.csumb.edu/SFMLwebDATA_c.htm) (March 2012).
- Catuneanu, O., 2006, *Principles of Sequence Stratigraphy*: Amsterdam, Elsevier, 375 p.
- Christie-Blick, N., and Biddle, K.T., 1985, Deformation and basin formation along strike-slip faults, in Biddle, K.T., and Christie-Blick, N., eds., *Strike-slip deformation, basin formation, and sedimentation*: Society of Economic Paleontologists and Mineralogists Special Publication 37, p. 1–34.
- Clark, D.H., Hall, N.T., Hamilton, D.H., and Heck, R.G., 1991, Structural analysis of late Neogene deformation in the central offshore Santa Maria Basin, California: *Journal of Geophysical Research*, v. 96, p. 6435–6457, doi:10.1029/90JB00922.
- Clark, P.U., Dyke, A.S., Shakun, J.D., Carlson, E., Clark, J., Wohlfarth, B., Mitrovica, J.X., Hostetler, S.W., and McCabe, A.M., 2009, The Last Glacial Maximum: *Science*, v. 325, p. 710–714, doi:10.1126/science.1172873.
- Crowell, J.C., 1974, Origin of late Cenozoic basins in southern California, in Dickinson, W.R., ed., *Tectonics and sedimentation*: Society of Economic Paleontologists and Mineralogists Special Publication 22, p. 190–206.
- Cunningham, W.D., and Mann, P., eds., 2007, *Tectonics of Strike-Slip Restraining and Releasing Bends*: Geological Society [London] Special Publication 290, 471 p.
- Dibblee, T.W., and Ehrenspeck, H.E., 1989, Geologic map of the Point Sal and Guadalupe quadrangles, Santa Barbara County, California: Dibblee Geological Foundation, Dibblee Foundation Map DF-25, scale 1:24,000.
- Dickinson, W.R., Ducea, M., Rosenberg, L.I., Greene, H.G., Graham, S.A., Clark, J.C., Weber, G.E., Kidder, S., Ernst, W.G., and Brabb, E.E., 2005, Net dextral slip, Neogene San Gregorio-Hosgri Fault Zone, coastal California: Geologic evidence and tectonic implications: *Geological Society of America Special Paper* 391, 43 p.
- Di Silvestro, L.A., Hanson, K.L., Lettis, W.R., and Shiller, G.I., 1990, The San Simeon/Hosgri pull-apart basin, south-central coastal California [abs.]: *Eos (Transactions, American Geophysical Union)*, v. 71, p. 1632.
- Draut, A.E., Hart, P.E., Lorensen, D.T., Ryan, H.F., Wong, F.L., Sliter, R.W., and Conrad, J.E., 2009, Late Pleistocene to Holocene sedimentation and hydrocarbon seeps on the continental shelf of a steep, tectonically active margin, southern California, USA: *Marine Geophysical Researches*, v. 30, p. 193–206, doi:10.1007/s11001-009-9076-y.
- Finlay, C.C., Maus, S., Beggan, C.D., Bondar, T.N., Chambodut, A., Chernova, T.A., Chulliat, A., Golovkov, V.P., Hamilton, B., Hamoudi, M., Holme, R., Hulot, G., Kuang, W., Langlais, B., Lesur, V., Lowes, F.J., Luhr, H., Macmillan, S., Manda, M., McLean, S., Manoj, C., Menvielle, M., Michaelis, I., Olsen, N., Rauberg, J., Rother, M., Sabaka, T.J., Tangborn, A., Toffner-Calussen, L., Thebaud, E., Thomson, A.W.P., Wardinski, I., Wei, Z., and Zvereva, T.I., 2010, International geomagnetic reference field, the eleventh generation: *Geophysical Journal International*, v. 183, p. 1216–1230, doi:10.1111/j.1365-246X.2010.04804.x.
- Greene, H.G., Maher, N.M., and Paull, C.K., 2002, Physiography of the Monterey Bay National Marine Sanctuary and implications about continental margin development: *Marine Geology*, v. 181, p. 55–82, doi:10.1016/S0025-3227(01)00261-4.
- Grossman, E.E., Eittreim, S.L., Field, M.E., and Wong, F.L., 2006, Shallow stratigraphy and sedimentation history during high-frequency sea-level changes on the central California shelf: *Continental Shelf Research*, v. 26, p. 1217–1239, doi:10.1016/j.csr.2006.04.001.
- Hall, C.A., 1973, Geologic map of the Morro Bay South and Port San Luis quadrangles, San Luis Obispo County, California: U.S. Geological Survey Miscellaneous Field Studies Map MF-511, scale 1:24,000.
- Hall, C.A., 1976, Geologic map of the San Simeon-Piedras Blancas region, San Luis Obispo County, California: U.S. Geological Survey Miscellaneous Field Studies Map MF-784, scale 1:24,000.
- Hall, C.A., Ernst, W.G., Prior, S.W., and Wiese, J.W., 1979, Geologic map of the San Luis Obispo-San Simeon region, California: U.S. Geological Survey Miscellaneous Investigations Series Map I-1097, scale 1:48,000.
- Hall, C.A., and Prior, S.W., 1975, Geologic map of the Cayucos-San Luis Obispo region, San Luis Obispo County, California: U.S. Geological Survey Miscellaneous Field Studies Map MF-686, scale 1:24,000.
- Hall, N.T., Hunt, T.D., and Vaughan, P.R., 1994, Holocene behavior of the San Simeon Fault Zone, south-central coastal California, in Alterman, I.B., McMullen, R.B., Cluff, L.S., and Slemmons, D.B., eds., *Seismotectonics of the central California Coast Ranges*: Geological Society of America Special Paper 292, p. 167–189.
- Hanson, K.L., and Lettis, W.R., 1994, Estimated Pleistocene slip rate for the San Simeon Fault Zone, south-central coastal California, in Alterman, I.B., McMullen, R.B., Cluff, L.S., and Slemmons, D.B., eds., *Seismotectonics of the central California Coast Ranges*: Geological Society of America Special Paper 292, p. 133–150.
- Hanson, K.L., Weslong, J.R., Lettis, W.R., Kelson, K.I., and Mezger, L., 1994, Correlation, ages, and uplift rates of Quaternary marine terraces, south-central coastal California, in Alterman, I.B., McMullen, R.B., Cluff, L.S., and Slemmons, D.B., eds., *Seismotectonics of the central California Coast Ranges*: Geological Society of America Special Paper 292, p. 45–71.
- Hanson, K.L., Lettis, W.R., McLaren, M.K., Savage, W.U., and Hall, N.T., 2004, Style and rate of Quaternary

- deformation of the Hosgri Fault Zone, offshore south-central California: U.S. Geological Survey Bulletin 1995-BB, 33 p.
- Hardebeck, J.L., 2010, Seismotectonics and fault structure of the California Central Coast: Bulletin of the Seismological Society of America, v. 100, p. 1031–1050, doi:10.1785/0120090307.
- Harding, T.P., 1985, Seismic characteristics and identification of negative flower structures, positive flower structures, and positive structural inversion: The American Association of Petroleum Geologists Bulletin, v. 69, p. 582–600.
- Hopson, C.A., 2007, Subvolcanic sheeted sills and non-sheeted dikes in ophiolites: Occurrence, origin, and tectonic significance for oceanic crust generation, in Cloos, M., Carlson, W.D., Gilbert, M.C., Liou, J.G., and Sorensen, S.S., eds., Convergent margin terranes and associated regions: A tribute to W.G. Ernst: Geological Society of America Special Paper 419, p. 225–254.
- Kern, J.P., 1977, Origin and history of upper Pleistocene marine terraces, San Diego, California: Geological Society of America Bulletin, v. 88, p. 1553–1566, doi:10.1130/0016-7606(1977)88<1553:OAHOU>2.0.CO;2.
- Langenheim, V.E., Jachens, R.C., and Moussauoi, K., 2009, Aeromagnetic survey map of the Central California Coast Ranges: U.S. Geological Survey Open-File Report 2009–1044, scale 1:250,000.
- Langenheim, V.E., Watt, J.T., and Denton, K.D., 2012, Magnetic map of the Irish Hills and surrounding areas, central California: U.S. Geological Survey Open-File Report 2012–1080, scale 1:24,000.
- Leslie, R.B., 1981, Continuity and tectonic implications of the San Simeon-Hosgri Fault Zone, central California: U.S. Geological Survey Open-File Report 81–430, 59 p.
- Lettis, W.R., DiSilvestro, L., Hanson, K.L., and Shiller, G.I., 1990, The San Simeon/Hosgri pull-apart basin: implications for late Quaternary activity on the Hosgri Fault Zone, in Lettis, W.R., Hanson, K.L., Kelson, K.I., and Wesling, J.R., eds., Neotectonics of the south-central coastal California: Friends of the Pleistocene, Pacific Cell, 1990 Fall Field Trip Guidebook, p. 91–138.
- Lettis, W.R., and Hall, N.T., 1994, Los Osos Fault Zone, San Luis Obispo County, California, in Alterman, I.B., McMullen, R.B., Cluff, L.S., and Slemmons, D.B., eds., Seismotectonics of the central California Coast Ranges: Geological Society of America Special Paper 292, p. 73–102.
- Lettis, W.R., Hanson, K.L., Unruh, J.R., McLaren, M.K., and Savage, W.U., 2004, Quaternary tectonic setting of southcentral coastal California: U.S. Geological Survey Bulletin 1995-AA, 21 p.
- Mann, P., 2007, Global catalogue, classification, and tectonic origin of restraining and releasing bends on active and ancient strike-slip fault systems, in Cunningham, W.D., and Mann, P., eds., Tectonics of strike-slip restraining and releasing bends: Geological Society [London] Special Publication 290, p. 13–142.
- McCaffrey, 2005, Block kinematics of the Pacific-North American plate boundary in the southwestern United States from inversion of GPS, seismological, and geologic data: Journal of Geophysical Research, v. 110, 27 p.
- McCulloch, D.S., 1987, Regional geology and hydrocarbon potential of offshore central California, in Scholl, D.W., Grantz, A., and Vedder, J.G., eds., Geology and resource potential of the Continental Margin of Western North America and adjacent oceans—Beaufort Sea to Baja California: Houston, Texas, Circum-Pacific Council for Energy and Mineral Resources, Earth Science Series, v. 6, p. 353–401.
- McHugh, C.M.G., Seeber, L., Cormier, M., Dutton, J., Cagatay, N., Polonia, A., Ryan, W.B.F., and Gorur, N., 2006, Submarine earthquake geology along the North Anatolia Fault in the Marmara Sea, Turkey: A model for transform basin sedimentation: Earth and Planetary Science Letters, v. 248, p. 661–684, doi:10.1016/j.epsl.2006.05.038.
- McLaren, M.K., Hardebeck, J.L., van der Elst, N., Unruh, J.R., Bawden, G.W., and Blair, J.L., 2008, Complex faulting associated with the 22 December 2003 Mw 6.5 San Simeon, California earthquake, aftershocks and postseismic deformation: Bulletin of the Seismological Society of America, v. 98, p. 1659–1680, doi:10.1785/0120070088.
- McLaren, M.K., and Savage, W.U., 2001, Seismicity of south-central coastal California: October 1987 through January 1997: Bulletin of the Seismological Society of America, v. 91, p. 1629–1658, doi:10.1785/0119980192.
- Meade, B.J., and Hager, B.H., 2005, Block models of crustal motion in southern California constrained by GPS measurements: Journal of Geophysical Research, v. 110, 19 p.
- Mitchum, R.M., Jr., Vail, P.R., and Sangree, J.B., 1977, Seismic stratigraphy and global changes of sea level, Part 6: Stratigraphic interpretation of seismic reflection patterns in depositional sequences, in Payton, C.E., ed., Seismic stratigraphy—Applications to hydrocarbon exploration: American Association of Petroleum Geologists Memoir 26, p. 117–134.
- Mix, A.C., Bard, E., and Schneider, R., 2001, Environmental processes of the ice age: Land, oceans, glaciers (EPILOG): Quaternary Science Reviews, v. 20, p. 627–657, doi:10.1016/S0277-3791(00)00145-1.
- Pacific Gas and Electric Company, 1988, Final report of the Diablo Canyon long-term seismic program: U.S. Nuclear Regulatory Commission Docket nos. 50–275 and 50–323.
- Peltier, W.R., 2005, On the hemispheric origins of meltwater pulse 1a: Quaternary Science Reviews, v. 24, p. 1655–1671, doi:10.1016/j.quascirev.2004.06.023.
- Petersen, M.D., Cao, T., Campbell, K.W., and Frankel, A.D., 2007, Time-independent and time-dependent seismic hazard assessment for the State of California: Uniform California Earthquake Rupture Forecast Model 1.0: Seismological Research Letters, v. 78, p. 99–109, doi:10.1785/gssrl.78.1.99.
- Petersen, M.D., Frankel, A.D., Harmsen, S.C., Mueller, C.S., Haller, K.M., Wheeler, R.L., Wesson, R.L., Zeng, B., Boyd, O.S., Perkins, D.M., Luco, N., Field, E.H., Wills, C.J., and Rukstales, K.S., 2008, Documentation for the 2008 update of the United States National Seismic Hazard Maps: U.S. Geological Survey Open-File Report 2008–1128, 61 p.
- Ryan, H.F., Parsons, T., and Sliter, R.W., 2008, Vertical tectonic deformation associated with the San Andreas Fault zone offshore of San Francisco, California: Tectonophysics, v. 457, p. 209–223.
- Sangree, J.B., and Widmier, J.M., 1977, Seismic stratigraphy and global changes of sea level, Part 9: Seismic interpretation of clastic depositional facies, in Payton, C.E., ed., Seismic stratigraphy—Applications to hydrocarbon exploration: American Association of Petroleum Geologists Memoir 26, p. 165–184.
- Sieh, K.E., and Jahns, R.H., 1984, Holocene activity of the San Andreas Fault at Wallace Creek, California: Geological Society of America Bulletin, v. 95, p. 883–896, doi:10.1130/0016-7606(1984)95<883:HAOTSA>2.0.CO;2.
- Sims, J.D., 1993, Chronology of displacement on the San Andreas Fault in central California: Evidence from reversed position of exotic rock bodies near Parkfield, California, in Powell, R.E., Weldon, R.J., III, and Matti, J.C., eds., The San Andreas Fault system: Displacement, palinspastic reconstruction, and geologic evolution: Geological Society of America Memoir 178, p. 231–256.
- Sliter, R.W., Triesenberg, P.J., Hart, P.E., Watt, J.T., Johnson, S.Y., and Scheirer, D.S., 2009, High resolution seismic-reflection and marine magnetic data along the Hosgri Fault Zone, central California: U.S. Geological Survey 2009–1100, v. 1.1: <http://pubs.usgs.gov/of/2009/1100/index.html> (March 2012).
- Sorlien, C.C., Kamerling, M.J., and Mayerson, D., 1999, Block rotation and termination of the Hosgri strike-slip fault, California, from three-dimensional map restoration: Geology, v. 27, p. 1039–1042, doi:10.1130/0091-7613(1999)027<1039:BRATOT>2.3.CO;2.
- Steritz, J.W., and Luyendyk, B.P., 1994, Hosgri Fault Zone, offshore Santa Maria Basin, in Alterman, I.B., McMullen, R.B., Cluff, L.S., and Slemmons, D.B., eds., Seismotectonics of the central California Coast Ranges: Geological Society of America Special Paper 292, p. 191–209.
- Swanson, M.T., 2005, Geometry and kinematics of adhesive wear in brittle strike-slip zones: Journal of Structural Geology, v. 27, p. 871–887, doi:10.1016/j.jsg.2004.11.009.
- Sylvester, A.G., and Darrow, A.C., 1979, Structure and new tectonics of the western Santa Ynez Fault system in southern California: Tectonophysics, v. 52, p. 389–405, doi:10.1016/0040-1951(79)90253-1.
- Titus, S.J., Dyson, M., DeMets, C., Tikoff, B., Rolandone, F., and Burgmann, R., 2011, Geologic versus geodetic deformation rates adjacent to the San Andreas Fault, central California: Geological Society of America Bulletin, v. 123, p. 794–820, doi:10.1130/B30150.1.
- U.S. Geological Survey (USGS), 2008, NAMSS: National Archive of Marine Seismic Surveys: <http://walrus.wr.usgs.gov/NAMSS/> (January 2012).
- U.S. Geological Survey (USGS), 2009, California Seafloor Mapping Program: <http://http://walrus.wr.usgs.gov/mapping/csmf/> (January 2012).
- U.S. Geological Survey and California Geological Survey, 2010, Quaternary fault and fold database for the United States: <http://earthquake.usgs.gov/hazards/qfaults/> (January 2012).
- Waelbroeck, C., Labeyrie, L., Michel, E., Duplessy, J.C., McManus, J.F., Lambeck, K., Balbon, E., and Labracherie, M., 2002, Sea-level and deep water temperature changes derived from benthic foraminifera isotopic records: Quaternary Science Reviews, v. 21, p. 295–305, doi:10.1016/S0277-3791(01)00101-9.
- Weber, G.E., 1994, Late Pleistocene slip rates on the San Gregorio Fault Zone at Point Año Nuevo, San Mateo County, California, in Lettis, W.R., ed., Field trip guidebook to transpressional deformation in the San Francisco Bay region: Friends of the Pleistocene, Pacific Southwest Cell.
- Wills, C.J., Weldon, R.J., II, and Bryant, W.A., 2008, Appendix A: California fault parameters for the National Seismic Hazard Maps and Working Group on California Earthquake Probabilities 2007: U.S. Geological Survey Open-File Report 2007–1437A, 48 p.
- Wright, J.D., 2000, Global climate change in marine stable isotope records, in Noller, J. S., Sowers, J. M., and Lettis, W. R., eds., Quaternary geochronology: Methods and applications: American Geophysical Union, p. 427–433.
- Yoshioka, T., 1996, Evolution of fault geometry and development of strike-slip basins: Comparative studies on the transform zones in Turkey: The Island Arc, v. 5, p. 407–419, doi:10.1111/j.1440-1738.1996.tb00162.x.